



# Endothelial cell supplementation promotes xenograft revascularization during short-term ovarian tissue transplantation

Mariagiulia Spazzapan<sup>a,1</sup>, Silvia Pegoraro<sup>b</sup>, Roman Vuerich<sup>a,c</sup>, Gabriella Zito<sup>b</sup>,  
Andrea Baldui<sup>b</sup>, Elena Longo<sup>d</sup>, Lorella Pascolo<sup>b</sup>, Miriam Toffoli<sup>e</sup>, Giorgia Meshini<sup>e</sup>,  
Alessandro Mangogna<sup>b</sup>, Gloria Ros<sup>f</sup>, Francesca Buonomo<sup>b</sup>, Federico Romano<sup>b</sup>,  
Letizia Lombardelli<sup>g</sup>, Giovanni Papa<sup>e</sup>, Marie-Pierre Piccinni<sup>g</sup>, Serena Zacchigna<sup>c,e</sup>,  
Chiara Agostinis<sup>b,\*</sup>, Roberta Bulla<sup>a,1</sup>, Giuseppe Ricci<sup>b,e,1</sup>

<sup>a</sup> Department of Life Sciences, University of Trieste, Trieste, Italy

<sup>b</sup> Institute for Maternal and Child Health, IRCCS Burlo Garofolo, Trieste, Italy

<sup>c</sup> Cardiovascular Biology Laboratory, International Centre for Genetic Engineering and Biotechnology (ICGEB), Trieste, Italy

<sup>d</sup> Elettra-Sincrotrone Trieste SCpA, Basovizza, Trieste, 34149, Italy

<sup>e</sup> Department of Medical, Surgical and Health Science, University of Trieste, Trieste, Italy

<sup>f</sup> Central RNA Laboratory, Istituto Italiano di Tecnologia (IIT), Genova, Italy

<sup>g</sup> Department of Experimental and Clinical Medicine, University of Florence, Florence, Italy

## ARTICLE INFO

### Keywords:

Ovarian tissue transplantation  
Endothelial cells  
Revascularization  
OTT mouse model

## ABSTRACT

The ischemic/hypoxic window after Ovarian Tissue Transplantation (OTT) can be responsible for the loss of more than 60 % of follicles. The implantation of the tissue supplemented with endothelial cells (ECs) inside dermal substitutes represents a promising strategy for improving graft revascularization. Ovarian biopsies were partly cryopreserved and partly digested to isolate ovarian ECs (OVECs). Four dermal substitutes (Integra®, made of bovine collagen enriched with chondroitin 6-sulfate; PELNAC®, composed of porcine collagen; Myriad Matrix®, derived from decellularized ovine forestomach; and NovoSorb® BMT, a foam of polyurethane) were compared for their angiogenic bioactive properties.

OVECs cultured onto the scaffolds upregulated the expression of angiogenic factors, supporting their use in boosting revascularization. Adhesion and proliferation assays suggested that the most suitable scaffold was the bovine collagen one, which was chosen for further *in vivo* experiments. Cryopreserved tissue was transplanted onto the 3D scaffold in immunodeficient mice with or without cell supplementation, and after 14 days, it was analyzed by immunofluorescence (IF) and X-ray phase contrast microtomography. The revascularization area of OVECs-supplemented tissue was doubled (7.14 %) compared to the scaffold transplanted alone (3.67 %). Furthermore, tissue viability, evaluated by nuclear counting, was significantly higher (mean of 169.6 nuclei/field) in the tissue grafted with OVECs than in the tissue grafted alone (mean of 87.2 nuclei/field).

Overall, our findings suggest that the OVECs-supplementation shortens the ischemic interval and may significantly improve fertility preservation procedures.

Peer review under the responsibility of editorial board of Bioactive Materials.

\* Corresponding author.

E-mail addresses: [MARIAGIULIA.SPAZZAPAN@phd.units.it](mailto:MARIAGIULIA.SPAZZAPAN@phd.units.it) (M. Spazzapan), [silvia.pegoraro@burlo.trieste.it](mailto:silvia.pegoraro@burlo.trieste.it) (S. Pegoraro), [Roman.Vuerich@icgeb.org](mailto:Roman.Vuerich@icgeb.org) (R. Vuerich), [gabriella.zito@burlo.trieste.it](mailto:gabriella.zito@burlo.trieste.it) (G. Zito), [abaldui@units.it](mailto:abaldui@units.it) (A. Baldui), [elena.longo@elettra.eu](mailto:elena.longo@elettra.eu) (E. Longo), [lorella.pascolo@burlo.trieste.it](mailto:lorella.pascolo@burlo.trieste.it) (L. Pascolo), [MIRIAM.TOFFOLI@phd.units.it](mailto:MIRIAM.TOFFOLI@phd.units.it) (M. Toffoli), [giorgia.meshini@gmail.com](mailto:giorgia.meshini@gmail.com) (G. Meshini), [alessandro.mangogna@burlo.trieste.it](mailto:alessandro.mangogna@burlo.trieste.it) (A. Mangogna), [gloria.ros@iit.it](mailto:gloria.ros@iit.it) (G. Ros), [francesca.buonomo@burlo.trieste.it](mailto:francesca.buonomo@burlo.trieste.it) (F. Buonomo), [federico.romano@burlo.trieste.it](mailto:federico.romano@burlo.trieste.it) (F. Romano), [letizia.lombardelli@unifi.it](mailto:letizia.lombardelli@unifi.it) (L. Lombardelli), [giovanni.papa@asugi.sanita.fvg.it](mailto:giovanni.papa@asugi.sanita.fvg.it) (G. Papa), [marie-pierre.piccinni@unifi.it](mailto:marie-pierre.piccinni@unifi.it) (M.-P. Piccinni), [zacchigna@icgeb.org](mailto:zacchigna@icgeb.org) (S. Zacchigna), [cagostinis@units.it](mailto:cagostinis@units.it) (C. Agostinis), [rbulla@units.it](mailto:rbulla@units.it) (R. Bulla), [giuseppe.ricci@burlo.trieste.it](mailto:giuseppe.ricci@burlo.trieste.it) (G. Ricci).

<sup>1</sup> These authors contributed equally to this work and share senior authorship.

<https://doi.org/10.1016/j.bioactmat.2025.03.021>

Received 13 March 2024; Received in revised form 14 March 2025; Accepted 26 March 2025

2452-199X/© 2025 The Authors. Publishing services by Elsevier B.V. on behalf of KeAi Communications Co. Ltd. This is an open access article under the CC BY-NC-ND license (<http://creativecommons.org/licenses/by-nc-nd/4.0/>).

## 1. Introduction

In the last decades, improved diagnosis and treatments for female prepubertal cancer patients have increased survival among reproductive-age women [1,2]. Most anti-cancer treatments are gonadotoxic, resulting in ovarian endocrine dysfunction and early depletion of ovarian reserve [2]. Furthermore, chemotherapeutics can damage both vascular networks and stromal cells and determine an early menopausal status [3]. Premature menopause not only negatively affects fertility potential but may also seriously impact the quality of life, increasing the risk of cardiovascular diseases, neurodegenerative pathologies, and osteoporosis [4]. Thus, fertility preservation represents a fundamental goal for the quality of life among young cancer survivors [5]. Both the American Society of Reproductive Medicine (ASRM) and the European Society of Human Reproduction (ESHRE) indicate embryo or oocyte cryopreservation as the first-line fertility preservation option [6,7]. Nevertheless, these methods display severe limitations: women need to be fertile, and ovarian stimulation for *in vitro* fertilization (IVF)/intracytoplasmic sperm injection (ICSI) may delay the start of anti-cancer treatments. Moreover, despite being an effective approach, embryo cryopreservation requires the presence of a male partner [8].

Ovarian Tissue Cryopreservation (OTC), followed by its transplantation (Ovarian Tissue Transplantation, OTT), is the only available option for prepubertal girls [9]. Since the first pregnancy resulting from this procedure in 2004 [10], conceiving and live birth rates have continued to climb steadily with an exponential increase, reaching more than 130 live births in June 2017 [2], and the number is currently expected to exceed 200 [11].

Revascularization is one of the key factors in ensuring a successful transplantation [12]. In fact, the hypoxic period after reimplantation lasts at least 5–7 days, and functional perfused blood vessels can be observed only after 7–10 days [2,13]. Regardless of the initial insult, the optimal healing of ischemic tissue depends on the balance between pro-inflammatory and pro-healing responses of innate immunity [14]. The ischemic window after OTT causes the loss of more than 60 % of follicles [15], requiring the development of novel strategies to reduce this interval.

Biomaterials used as 3D scaffolds are designed to replace and support damaged or diseased tissue regrowth. They are designed and synthesized to provide hope in overcoming challenges in reproductive tissue engineering. In the field of tissue engineering, some biomaterials can not only directly interact with biological organisms but also guide the reconstruction of the basic structure and morphology of organs, hastening tissue regeneration. Moreover, biomaterials are commonly supplemented with cells, growth factors, and drugs rather than used independently. This combination can significantly improve the long-term retention of cells in the body and serve as carriers for drugs and growth factors [16].

Over the last decades, several attempts have been performed to curtail the ischemic/hypoxic damage of auto-transplanted ovarian tissue, in particular the supplementation with different growth factors (e.g., Vascular Endothelial Growth Factor-VEGF [17], or basic Fibroblast Growth Factor-bFGF [18]), hormones (e.g., Human Menopausal Gonadotropin-HMG [19], or Anti-Müllerian Hormone-AMH [20]), or antioxidants (e.g., vitamin E [21], or N-acetylcysteine [22]). Furthermore, some groups have attempted to support OTT by using mesenchymal stem cells (MSCs), and particularly Adipose-Derived Stem Cells (ADSCs), due to their well-known anti-inflammatory and pro-angiogenic effects [23–25]. Numerous studies on murine animal models have indicated that adding human mesenchymal or bone marrow cells helps restore function to ovaries in premature ovarian failure [26–29]. Since graft resident endothelium is essential for tissue recovery after transplantation, the supplementation of grafts with an autologous source of endothelial cells (ECs) before transplantation, a procedure known as inosculation [30], may be a promising approach to reduce the ischemic/hypoxic period.

The use of commercially available specialized matrices has been widely explored in regenerative medicine to develop novel biomaterials for reproductive tissue engineering [16,31,32]. In 2016, Oktay *et al.* reported the first live birth after the transplantation of frozen ovarian tissue combined with a scaffold [33]. In the field of tissue bioengineering, the scaffold serves as a template in which cells and/or growth factors are implanted to reproduce the extracellular matrix (ECM) features. For this reason, a suitable scaffold should possess several characteristics, such as high porosity, pore interconnectivity, biocompatibility, biodegradability, mechanical properties, non-toxic and non-immunogenic properties, along with antifungal, antibacterial, and antitumor properties [34].

In the context of revascularization, studies on the application of 3D scaffolds to wound healing are well-established. A skin substitute works as a scaffold stimulating the synthesis of new dermal tissue, allowing host cells to proliferate, delivering or augmenting the production of cytokines and growth factors [35].

In the current study, we tested four different dermal substitutes (*i.e.*, Integra® Bilayer Matrix Wound Dressing, PELNAC®, Myriad Matrix®, and NovoSorb® BTM) for their ability to induce pro-angiogenic responses. Integra® is a two-layer system: the outer layer is a silicone membrane that covers a three-dimensional matrix made of cross-linked bovine collagen type I (80 µm diameter mean pore size) with the addition of shark chondroitin sulfate, a glycosaminoglycan [36,37]. PELNAC® is a bilaminar sponge made of cross-linked pig atelocollagen (85 µm diameter mean pore size), covered by a silicone film layer [37,38]. Myriad Matrix® derives from decellularized propria submucosa isolated from ovine forestomach tissue [39]. It retains the native collagen structure of normal tissue ECM, as well as more than 150 functional secondary molecules crucial for cell adhesion, migration, proliferation, and rapid development of capillary networks [40]. Lastly, NovoSorb® BMT is a synthetic dermal matrix composed of a biodegradable foam of polyurethane (188 µm diameter mean pore size) with an overlying temporary non-biodegradable polyurethane membrane [41].

Since the revascularization process is one of the key aspects, using a pre-vascularized scaffold may have a crucial impact on the engraftment success rate [42]. We previously demonstrated that the interaction between ECs and the most widely used dermal substitutes induced the expression of multiple angiogenic factors by ECs. Furthermore, dermal substitutes combined with ECs promoted engraftment and vascularization *in vivo*, suggesting that this approach may represent a promising strategy for tissue revascularization [43]. In this work, we propose the development of an Advanced Therapeutic Medicinal Product (ATMP) combining the ovarian tissue with a dermal substitute, used as a 3D scaffold inosculation with ovarian ECs (OVECs) in order to reduce the ischemic window and improve graft survival and tissue viability. Using an *in vivo* mouse model of ovarian xenograft, we evaluated whether adding autologous human EC could increase the vascularization of the transplanted tissue using 3D scaffolds as a biologically active “sponge” to cell application and transplanted tissue support. The 3D scaffold was chosen among clinically used dermal substitutes based on its pro-adhesive, pro-proliferative, and pro-angiogenic characteristics on ovarian ECs. The evaluation of the increase in vascularization on the excised tissues was analyzed using various techniques, including confocal immunofluorescence (IF) and X-ray microtomography.

## 2. Materials and methods

### 2.1. Reagents and antibodies

The following antibodies were used: mouse mAb anti-human CD34 (#MA5-15331), Alexa Fluor 647 donkey anti-mouse IgG (H + L) (#A-31571), Alexa Fluor 594 donkey anti-goat IgG (H + L) (#A-11058), and Alexa Fluor 488 donkey anti-rabbit IgG (H + L) (#A-21206) were purchased from ThermoFisher Scientific (Massachusetts, USA); rabbit mAb anti-human CD31/PECAM1 (#ZRB1216) from Sigma-Merck (Missouri,

USA); mouse mAb anti-human von Willebrand Factor (vWF; #M0616), rabbit pAb anti-human vWF (#IS527), rabbit pAb anti-human CD34 (#Qbend10), rabbit mAb anti-human CK8/18 (#M3652), mouse mAb anti-human CD31/PECAM1 (#M0823), mouse anti-human CD68 (#14-0688-80), and goat anti-mouse FITC-conjugated F(ab)' (#F0479) from Dako (Milan, Italy); mouse mAb anti-human podoplanin (#MABT855) was bought from Abcam (Cambridge, UK); mouse mAb anti-human VE-cadherin was obtained through the courtesy of Prof. Dejana (Mario Negri Institute, Milan, Italy); goat mAb anti-mouse CD31/PECAM-1 (#AF3628) from R&D Systems (Minnesota, USA); rabbit pAb anti-NG2 Chondroitin Sulfate Proteoglycan (#AB5320) was purchased from Merck (Darmstadt, Germany); goat anti-rabbit FITC-conjugated (#11-4839-81) was purchased from Jackson ImmunoResearch (Milan, Italy); mouse anti-human CD31 FITC-conjugated (#557508) was bought from BD Bioscience (New Jersey, USA); anti-rabbit Horseradish Peroxidase (HRP) conjugated (#A120-113P) was bought from Fortis Life Sciences (Massachusetts, USA), while chicken anti-mouse HRP-conjugated (#AP126P) from Sigma-Merck.

All chemicals were purchased from Sigma-Merck.

2.2. Matrices

Four different Acellular Dermal Matrices (ADMs) were tested, and their features are listed in Table 1. Briefly, the matrices compared were:

- Integra® Bilayer Matrix Wound Dressing (named bovine collagen; Integra Life Sciences Corporation, Plainsboro, NJ, USA), composed of cross-linked bovine collagen type I and shark chondroitin-6-sulfate with a silicone layer [44–46];
- PELNAC® (named porcine collagen; Gunze Corp., Osaka, Japan), which is a bilaminar membrane composed of a silicone film layer and a porcine tendon collagen sponge layer [37];
- Myriad Matrix® (named D.O.F.; AROA BIOSURGERY, Auckland, New Zealand), a collagen matrix derived from decellularized ovine forestomach, which maintains biological structure and functions of the ECM [40,47];
- NovoSorb® BTM (named P-U; Polynovo, Melbourne, Australia), which is made of biodegradable polyurethane [48].

2.3. Patient enrollment

Ovarian samples were obtained from patients undergoing ovariectomy/adnexectomy during sex reassignment surgery or patients suffering from benign gynecological diseases unrelated to ovaries (e.g., leiomyomas). Patients (n = 17) were enrolled at the Institute for

Maternal and Child Health, IRCCS Burlo Garofolo (Trieste, Italy), after signing an informed consent form (Supplementary Table S1). Patients were divided into two main categories: patients manifesting Gender Dysphoria [G.D., n = 8; mean age = 28.6 years old (y), standard deviation (SD) = 5] and patients undergoing ovariectomy/adnexectomy for other benign gynecological diseases (n = 9; mean age = 51.3 y, SD = 11.6). The study was reviewed and approved by the Regional Ethical Committee of FVG (CEUR, Udine, Italy; prot. 0010143/P/GEN/ARCS 2019). Tissues were cut in three parts: the first one was sliced for tissue cryopreservation, the second part was minced for cell isolation, and the latter was fixed in 10 % buffered formalin, paraffin-embedded, and stored at 4 °C for immunohistochemical evaluation (Supplementary Fig. S1).

2.4. Immunohistochemical analysis

Sections were deparaffinized and rehydrated. Antigen retrieval was performed in Tris-HCl/EDTA buffer, pH 9, for 20 min at 95 °C. Endogenous peroxidases were inhibited with 3 % v/v H<sub>2</sub>O<sub>2</sub> for 5 min. Sections were then incubated with dPBS +1 % horse serum for 30 min to block unspecific binding, followed by incubation with anti-human vWF (1:300) or anti-human CD34 (1:300) overnight (ON) at 4 °C. After washing the sections, anti-rabbit horseradish peroxidase (HRP)-conjugated (1:500) or anti-mouse HRP-conjugated (1:250) were incubated for 30 min at room temperature (RT), prior to detection by using AEC kit (Vector Laboratories). Sections were counterstained with Mayer's hematoxylin (DiaPath) and examined under a Leica DM 2000 optical microscope. Images were collected using a Leica DFC 7000 T digital camera (Leica Microsystems, Wetzlar, Germany).

2.5. Vitrification and thawing of ovarian tissue

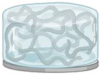



The cryopreservation of ovarian tissue slices was performed following the instructions of the MediCult Vitrification Cooling kit (CooperSurgical Fertility Companies, Trumbull, Connecticut, USA). Briefly, the ovarian slices were incubated for 30 min at RT with Equilibrium Medium containing 7.5 % v/v ethylene glycol (EG) and 7.5 % v/v 1–2 propanediol (PROH). Then, samples were transferred to Vitrification Medium (15 % v/v EG, 15 % v/v PROH, and 0.5M sucrose). After 20 min at RT, the slices were directly placed in liquid nitrogen, then transferred to a pre-cooled cryovial, and stored in liquid nitrogen.

The thawing procedure was conducted following the instructions of the MediCult Vitrification Warming kit (CooperSurgical Fertility Companies, Trumbull, Connecticut, USA). Cryovials were kept for 40 s at RT before placing the ovarian slices in the Thawing Medium containing 1M sucrose for 1 min at 37 °C. Samples were then transferred in Diluent Medium I, with 0.5M sucrose, for 3 min, and subsequently in Diluent Medium II, with 0.25M sucrose. After 3 min in Diluent Medium II, ovarian tissues were washed thrice in Washing Medium for 3 min (each washing step). Eventually, ovarian slices were employed for *in vivo* experiments or fixed for morphological analyses.

2.6. Cell isolation and culture

Ovarian Endothelial Cells (OVECs) were isolated from ovarian samples collected as mentioned above. Ovarian biopsies were minced into small pieces. After a first digestion in 0.1 % trypsin, the solution was replaced by 3 mg/ml collagenase type I. The positive selection of OVECs was performed by using a mixture of Dynabeads® CD31 and UEA-lectin (Ulex Europeus Agglutinine-Lectin)-conjugated magnetic beads. Positive cells were seeded on a fibronectin-gelatin coated flask and cultured in Human Endothelial Serum Free Medium (HESFM; Gibco, Carlsbad, CA) supplemented with 20 ng/mL bFGF, 10 ng/mL Epidermal Growth Factor (Immunological Sciences), 1 % penicillin-streptomycin (Sigma-Merck), 10 % v/v fetal bovine serum (FBS; Life Technologies), 10 % v/v human serum (Sigma-Merck), and 1 µg/mL hydrocortisone (Sigma-Merck).

**Table 1**  
Schematic representation of the tested Acellular Dermal Matrices.

Commercial Name	Scaffold Name	Image	Composition
Integra® Bilayer Matrix Wound Dressing	Bovine coll.		Silicone film layer Bovine tendon collagen type I Shark chondroitin-6-sulfate
PELNAC®	Porcine coll.		Silicone film layer Porcine tendon collagen sponge layer
Myriad Matrix®	D.O.F.		Decellularized Ovine Forestomach
NovoSorb® BTM	P-U		Polyurethane

Adapted from Agostinis et al. [43].

Cells were maintained in culture at 37 °C in a 5 % v/v CO<sub>2</sub> incubator, in a humidified atmosphere, and split about every 72 h.

## 2.7. Immunofluorescence

Cells were seeded onto 8-chamber culture slides (Corning, New York, USA) pre-coated with fibronectin (2 µg/cm<sup>2</sup>). Confluent cells were fixed with 1 % paraformaldehyde (PFA) for 15 min in the dark. In order to perform quenching, blocking, and permeabilization, cells were incubated with a solution of 1 % BSA (Bovine Serum Albumin), 0.1 % Triton X-100, and 50 mM glycine in dPBS (Dulbecco's Phosphate Saline Buffer, Sigma Aldrich) for 30 min at RT. Anti-human CD31/PECAM1 (1:50), anti-human vWF (1:50), anti-human VE-cadherin (1:2), or anti-human CD34 (1:100) diluted in dPBS-2 % BSA-0.7 mM Ca<sup>2+</sup>-0.7 mM Mg<sup>2+</sup> were added for 1 h at RT. Then, anti-rabbit (1:500) or anti-mouse FITC-conjugated (1:300) secondary antibodies were incubated for 30 min at RT. Nuclei were stained with DAPI. Glass slides were mounted with a Fluorescence Mounting Medium (Dako), and images were acquired with Leica DM3000 microscope (Leica, Wetzlar, Germany) using a Leica DFC320 digital camera (Leica).

For *in vivo* experiments, samples were retrieved and fixed in 2 % PFA at 4 °C ON. Tissues were then equilibrated in 30 % sucrose at 4 °C ON, before embedding in OCT (Bio-Optica). Sections were permeabilized with 0.5 % v/v Triton X-100 in dPBS for 20 min, and blocked in 5 % BSA in dPBS for 1 h. Samples were incubated ON at 4 °C with the primary antibody diluted 1:100 in 1 % BSA-0.1 % Tween-20 in dPBS. Subsequently, secondary antibodies were diluted 1:500 in 1 % BSA-0.1 % Tween-20 in dPBS for 2 h at RT. Nuclei were counterstained with DAPI. Slides were mounted using Mowiol mounting medium. Images were acquired with a Nikon Eclipse Ti-E inverted fluorescent microscope equipped with DC-152Q-C00-FI using NIS V4.30 software (Nikon) and a ZEISS LSM 880 with Airyscan. For each sample, at least four images were acquired. Images were analyzed using ImageJ2 (Fiji) software. Z projection was performed at maximum intensity. Stitched images were acquired using NIS V4.30 software (Nikon).

## 2.8. Flow cytometry

Cells (5x10<sup>5</sup>) were fixed in 3 % PFA for 15 min in the dark. Next, they were incubated with anti-human CD31/PECAM1-FITC (1:25), anti-human vWF (1:50), or anti-human CK8/18 (1:50) diluted in saponin A (Farmitalia Carlo Erba, Milan, Italy) for 45 min on ice. Incubation with FITC-conjugated secondary antibodies was performed for 30 min on ice in the dark. Cells were resuspended and fixed in 1 % PFA. Fluorescence was acquired with Attune NxT Flow Cytometer (ThermoFisher Scientific), and data were processed using Attune Cytometric v6.0 Software (ThermoFisher Scientific).

## 2.9. Adhesion assay

Scaffolds (bovine collagen, porcine collagen, D.O.F., and P-U) were cut into small pieces (8 mm in diameter) using a biopsy punch in sterile conditions. Before seeding, cells were stained with 10 µg/mL of the fluorescent dye FAST DiI (Molecular Probes, Invitrogen) diluted in dPBS. After 15 min at 37 °C in a 5 % v/v CO<sub>2</sub> incubator, cells (2.5x10<sup>5</sup>) were resuspended in HESFM supplemented with 10 % FBS and hydrocortisone, and seeded onto the scaffolds. After 5, 15, or 30 min at 37 °C in a 5 % v/v CO<sub>2</sub> incubator, non-adherent cells were removed by washing with dPBS-0.7 mM Ca<sup>2+</sup>-0.7 mM Mg<sup>2+</sup>. Cells were lysed, and fluorescence was immediately measured using Infinite200 (TECAN Italia, Milan, Italy).

## 2.10. Proliferation assay

Cells (1.5x10<sup>5</sup>) were seeded onto bovine or porcine collagen cut with a biopsy punch (8 mm of diameter) or onto a coating of fibronectin in a

24-well plate (Corning), and cultured in HESFM + 10 % FBS + hydrocortisone at 37 °C in a 5 % v/v CO<sub>2</sub> incubator. After 72 h, CellTiter 96® AQueous One Solution Reagent (Promega, Wisconsin, USA) was added and incubated for 1 h. Absorbance was read at 490 nm using a plate reader spectrophotometer (PowerWaveX, Bio-Tek Instruments).

## 2.11. A1R MP confocal multiphoton microscope (Nikon) acquisition

OVECs (9x10<sup>5</sup>) were seeded onto bovine collagen for 1 h (t0) to allow cell adhesion to the scaffold or for 48 h (t48). Then, cells were fixed with 3 % PFA and stained with phalloidin-FITC (1:25, Invitrogen, ThermoFisher Scientific). Nuclei were stained with Hoechst (ThermoFisher Scientific). Images were acquired with A1R MP confocal multiphoton microscope (Nikon).

## 2.12. Real-time quantitative PCR

OVECs were cultured for 48 h onto bovine collagen, porcine collagen, or in 2D condition (fibronectin). RNA was isolated by using TRIzol™ Plus RNA Purification Kit (ThermoFisher Scientific), and RNA quantification was performed via NanoDrop® spectrophotometer (Life Real). RNA was converted to cDNA using SensiFAST™ cDNA Synthesis Kit (Meridian Bioscience, Memphis, TN, USA), as previously described [49]. The expression level of the following genes was evaluated: *VEGF-A*, *PGF*, *ANGPT1*, *SEMA3A*, *KDR*, *FLT1*, *NRP1*, *TEK*, *MMP2*, *IL6*, and *IL8*. The sequences of the primers used are included in [Supplementary Table S2](#). The reaction was performed by the Rotor-Gene 6000 (Corbett, Explera), via 40 cycles made up of two steps: the denaturation step (10 s at 95 °C) and the combined annealing and amplification step (40 s at 60 °C, melting temperature of the primers). The expression level of the genes was then evaluated via comparative quantification by Rotor Gene 1.7 Software (Corbett Research) and normalized with the expression of the housekeeping genes (*GAPDH* and *TBP*) [50]. Data for genes that were not detectable (ND) were expressed as the Ct value of the housekeeping gene (*TBP*) and the target genes (*TNF*, *MMP9*, and *MCPI/CCL2*). A positive control of gene expression was used to monitor the PCR reaction.

## 2.13. In vivo OTT model

Ovarian biopsies were partially cut into organotypic tissue slices (800–1700 µm of thickness) with a slicer Leica vibratome VT1200 S and then vitrified. OVECs (2.5x10<sup>5</sup>) were resuspended in HESFM and seeded for 30 min at 37 °C, 5 % v/v CO<sub>2</sub>, onto bovine collagen previously cut into small pieces (8 mm in diameter). In the meantime, frozen ovarian tissue was thawed as previously described. Then, the tissue was placed onto the scaffold, with or without OVECs, and the ATMP was implanted on the back of immunodeficient NOD SCID gamma (NSG) mice under general anesthesia by intraperitoneal injection of ketamine (100 mg/kg)/xylazine (10 mg/kg). The skin was opened with a 10 mm longitudinal incision using scissors. A 2 × 2 cm pocket was formed with blunt dissection, and the scaffolds were applied with the cells facing down. The incision was closed with a 5–0 suture thread. Institutional guidelines in compliance with national and international laws and policies were followed for animal care and treatments. All experimental procedures were approved by the ICGEB Animal Welfare Board, with the requirements of the EU Directive 2010/63/EU, and by the Italian Ministry of Health. After 2 weeks, the mice were sacrificed by cervical dislocation after anesthesia with 5 % isoflurane. ATMPs and the surrounding tissue were collected, transversely cut in half, and fixed ON using 2 % v/v PFA in dPBS solution (Santa Cruz), for immunofluorescence (IF), or in 10 % buffered formalin, paraffin-embedded and stored at 4 °C, for immunohistochemistry (IHC) and X-ray phase-contrast microtomography.



## 2.14. Quantification by Multiplex Gene Assay (Quantigene 2.0) of mRNA for AMH

Quantigene™ 2.0 technique is a multiplex platform allowing the simultaneous analysis of several target RNA molecules (up to 80) present in a single sample. Quantigene Assays use an accurate method for multiplexed or single gene expression quantitation. The mRNA quantization for the genes was performed with a Multiplex Gene Assay (Thermo Fisher, MA, USA), as previously described elsewhere [51,52]. Briefly, the mRNA expression of *AMH* and *ACTB* (high expression housekeeping gene) was measured using the Quantigene multiplex assay (Thermo Fisher, MA, USA). Ovary samples were frozen in RNA later (Qiagen, Germany). Each sample was weighed, and the appropriate lysis solution was added to a final volume of 150  $\mu$ L containing 50 % Lysis Mixture and 1 g/L Mixture (Thermo Fisher, MA, USA) and 1 g/L proteinase K. The mixture was shaken at 65 °C for 30 min to lyse the cells. The lysate was stored at –80 °C for later use.

A panel of oligonucleotide capture probes, each with a unique sequence of 15 bases, was covalently linked to carboxylated fluorescently encoded beads (Luminex, Bio-rad, Massachusetts, USA). We mixed each sample lysate diluted at 1:1 and 1:2 with the pooled capture beads in a round-bottom assay well and hybridized for 16 h at 54 °C (the final volume in each well was 100  $\mu$ L). The assay mixture was transferred to a MultiScreen filter plate (Millipore, Billerica, MA, USA), and unbound material was filter-washed from the wells by rinsing 3 times with wash buffer. The plate was then hybridized at 54 °C for 1 h with 100  $\mu$ L/well of bDNA amplifier in Amplifier Diluent (Thermo Fisher, MA, USA). Then the plate was filter-washed twice with wash buffer and incubated at 50 °C for 1 h with 100  $\mu$ L/well of 5'-dT (Biotin)-conjugated label probe (Thermo Fisher, MA, USA) diluted in Label Probe Diluent (Thermo Fisher, MA, USA). After 2 washes, streptavidin-conjugated R-phycoerythrin diluted in SA-PE diluent (20 mmol/L Tris-HCl, 400 mmol/L lithium chloride, 1 mL/L Tween 20, 1 mL/L bovine serum albumin, and 5 mL/L Micr-O-protect) was added, and the plate was shaken and incubated at room temperature for 30 min. We washed the beads to remove unbound SA-PE and then analyzed them with Bio-Plex 200 system (Bio-Rad). The SA-PE fluorescence measured from each bead was proportional to the number of mRNA transcripts captured by the beads. Expression of target-specific RNA molecules was normalized against *ACTB* gene (high expression housekeeping gene).

## 2.15. X-ray phase-contrast microtomography

Paraffin-embedded tissues were imaged by X-ray phase-contrast microtomography (microCT) at SYRMEP (SYnchrotron Radiation for MEDical Physics) beamline of Elettra-Sincrotrone S.C.p.A. (Trieste, Italy) [53]. Some samples were stained by incubation for 2 h in a 1 % w/v iodine alcoholic solution (70 %) prior to paraffin inclusion [54]. The investigation was performed with the high-resolution white/pink beam setup in parallel geometry. The images were acquired at an average energy of 16.7 keV, after filtering the beam with a 0.5 mm-thick silicon filter, while the electron storage ring was operating at 2.0 GeV. Samples without iodine were imaged at a sample-to-detector distance of 15 cm, while samples prepared with iodine contrast agent at 10 cm. A Hamamatsu sCMOS camera (2048 x 2048 pixels, pixel size: 6.5  $\mu$ m x 6.5  $\mu$ m) coupled to a 17  $\mu$ m-thick GGG scintillator screen was used for image collection. Thanks to an optical magnification system connected to the detector, the effective pixel size selected for the tomographic acquisition was 0.9  $\mu$ m x 0.9  $\mu$ m, thus resulting in a field of view of 1.8 mm x 1.8 mm out of 180° microCT scans. For the specimen with cells and not injected with iodine specifically, the field of view was further increased to approximately 3.3 mm x 3.3 mm by a 360 degrees off-axis tomography scan. All images were collected with 100 ms exposure time. Tomography datasets accomplished over 180° comprised 1800 projections, while 360° scans were obtained by collecting 3600 projections. Moreover, 20 dark images and 20 flat images (i.e., images of the background)

were acquired at the beginning of each measurement. Raw data were processed using Syrmep Tomo Project (STP) software [55]. First, the projections were normalized by conventional flat-fielding, and potential ring artifacts were attenuated with dedicated ring removal filters available in STP. Then, the projections were phase retrieved by Paganin's algorithm [56]. Delta/beta ratio was tuned to enhance the visualization of specific anatomic features. Samples with iodine were retrieved with a delta/beta ratio of 20, the control sample without iodine was processed with a delta/beta of 100, and the tissue with cells and without iodine with a ratio of 350. Finally, virtual sections in 32-bit were reconstructed by applying Filtered Back Projection algorithm in combination with Shepp-Logan filter. All reconstructed volumes were down-converted into 16-bit images using an in-house python script. The images of the tissues were further treated with the unsharp filter (radius equal to 3, sigma equal to 0.60) available in the open-source software Fiji. All datasets were visually inspected by Fiji and compared with the corresponding histological slices. The representation of the orthogonal views was prepared by Avizo 3D software (version 2021.1).

## 2.16. Statistical analyses

Data are represented as mean  $\pm$  standard error of the mean (SEM). Statistical analyses were performed by using the GraphPad Prism 9 software (GraphPad Software, San Diego, USA). The normal distribution of datasets was tested and, depending on the results, multiple comparisons were performed with the parametric one- or two-way analysis of variance (ANOVA), while single comparisons were analyzed with the nonparametric Mann–Whitney test or the parametric one-tailed *t*-test. Results with *p*-value (*p*) < 0.05 were considered statistically significant.

## 3. Results and discussion

### 3.1. Histological evaluation of ovarian tissue vascularization and characterization of OVECs

Reducing the ischemic/hypoxic window after ovarian tissue autotransplantation is still a challenging clinical need in reproductive medicine. A vascular cell-based strategy may accelerate the perfusion of ovarian tissue and mitigate ischemia. Thus, we first evaluated the vascularization levels of ovarian tissues collected from patients undergoing ovariectomy/adnexectomy. Ovarian vascularization is complex [57], as illustrated in [Supplementary Fig. S2](#).

Albeit the ovarian samples were mainly obtained from testosterone-treated G.D. patients, histochemical and immunohistochemical analyses revealed the presence of several follicles ([Fig. 1a](#)), predominantly primordial or primary follicles. Secondary/antral follicles were also observed in a few samples ([Supplementary Fig. S3](#)). These findings support the hypothesis that almost one-third of G.D. patients still ovulate, despite being amenorrheic [58]. Furthermore, IHC staining for the endothelial markers vWF ([Fig. 1b and c](#)) and CD34 ([Fig. 1d and e](#)) revealed abundant vascularization. In fact, previous studies demonstrated that the oocyte itself, and granulosa and theca cells as well, can produce VEGF during follicle maturation to support the need for oxygen and nutrients [59–61]. The tissues were incubated with secondary antibodies alone to exclude any non-specific/background staining ([Supplementary Fig. S4](#)).

Due to the pivotal involvement of ECs in revascularization processes, we aimed first to set up a novel protocol to successfully isolate ECs from ovarian tissues. After mechanical, trypsin, and collagenase digestion, OVECs were positively selected via magnetic beads conjugated with endothelium-specific markers, as summarized in [Fig. 1f](#). Freshly isolated OVECs were characterized by IF for the presence of endothelial (CD31/PECAM-1, vWF, VE-cadherin, and CD34), lymphatic (podoplanin), epithelial (CK8/18), and macrophage lineage (CD68) markers, revealing a high purity level of the endothelial population ([Fig. 1g and Supplementary Fig. S5](#)). Cytofluorimetric analyses ([Fig. 1h](#)) confirmed that the

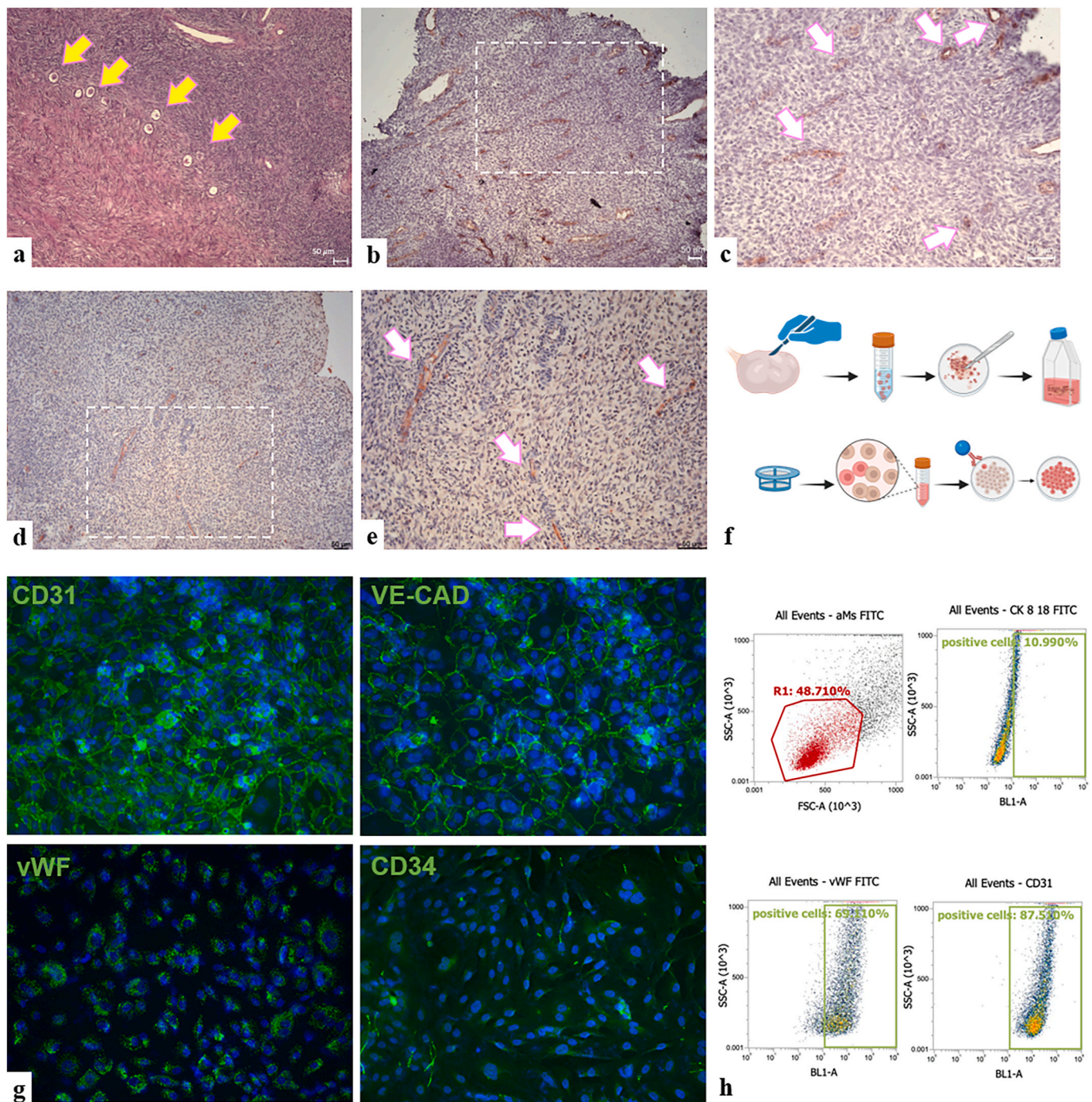


**Fig. 1. Histological and immunohistochemical evaluation of ovarian tissue and characterization of isolated OVECs.** The presence of primordial/primary follicles was assessed by hematoxylin/eosin (a). Vessels were revealed by staining for vWF (b,c) and CD34 (d,e). (c,e) Zoomed fields of IHC staining showing a representative figure of 1 section out of 5 ovarian tissue samples ( $n = 5$ ). AEC (red) chromogen was used to visualize the binding of anti-human vWF and anti-human CD34. Nuclei were stained with Mayer's Hematoxylin. Yellow arrows indicate ovarian follicles; white arrows indicate ovarian vessels. Magnification, 10 $\times$  (a,b,d); 20 $\times$  (c,e). Scale bars, 50  $\mu$ m. Schematic representation of OVEC isolation protocol (f) and characterization for endothelial markers by IF (g). Cells were grown to confluence in eight-chamber culture slides. After fixation and permeabilization, cells were stained with mAb anti-human CD31/PECAM-1, VE-cadherin, vWF, and CD34, followed by anti-mouse-Alexa Fluor<sup>TM</sup> 488 or anti-rabbit-Alexa Fluor<sup>TM</sup> 488 secondary antibodies. Nuclei were stained by DAPI (blue). Original magnification, 20 $\times$ . The same antibodies were used to confirm IF results by flow cytometry. Representative results of cytofluorimetric analyses (h) for CD31/PECAM-1, vWF, and CK8/18, or secondary antibodies only (anti-mouse FITC).

population was almost 90 % composed of ECs. In particular, cells resulted in 88.1 % positive for CD31/PECAM-1, 88.6 % for vWF, and 10.3 % for CK8/18.

### 3.2. Interaction between OVECs and ADMs increases cell adhesion and proliferation

We previously demonstrated that using solid biomaterials is the optimal strategy for cellular implementation [24]. Thus, we attempted to identify the best-performing 3D scaffold pre-seeded with OVECs by



comparing four commercial ADMs, already tested in our previous study [43] (Table 1).

Adhesion assays demonstrated that cells could adhere quickly to all the scaffolds, although at different levels. The highest percentage of adherent cells was observed onto bovine collagen, whereas adhesion was significantly lower onto the other three scaffolds. In addition, the percentage of adherent cells remained almost stable along the three time points investigated (Fig. 2a). Our results indicated that the bovine collagen scaffold displayed the best pro-adhesive properties in comparison with the other ADMs and were consistent with our previous findings on ECs isolated from skin biopsies (Adult Dermal Microvasculature Endothelial Cells, ADMECs) [43], probably due to its glycosaminoglycane crosslinked structure (Table 1).

As a further step, we evaluated the capability of the scaffolds to induce cell proliferation. Cells were seeded onto bovine or porcine collagen scaffold (the most frequently used ADMs), or fibronectin (control condition), assessing cell viability after 72 h. MTS assay revealed higher cell proliferation onto the scaffolds as compared to the 2D condition (Fig. 2b), suggesting that their use in tissue transplantation could actively increase the successful rate of OTT. Based on these results and consistently with our previous observations in ADMECs [43], further analyses were limited to bovine and porcine collagens only.

Since no information is currently available about the profile of cell colonization and organization inside the scaffolds, we also monitored cell viability by multiphoton microscopy. Cells were seeded onto the bovine collagen scaffold, fixed, and then stained after 1 h and 48 h. Hoechst staining was used to visualize the nuclei and spatially investigate cell deepening into the matrix, while the cytoskeletal component F-actin allowed us to appreciate cell-scaffold contacts. 2D projections of the nuclei revealed an increase in the number of OVECs after 48 h, compared to 1 h (Fig. 2c–Supplementary Video S1, after 1 h, and Supplementary Video S2, after 48 h), confirming previous proliferation data. Moreover, cell colonization seemed to involve the entire matrix thickness. Phalloidin staining highlighted the maintenance of a rounded cell shape after 1 h, whereas after 48 h, OVECs assumed a spread-out morphology (Fig. 2d). These observations were also confirmed by the 3D reconstruction (Fig. 2e and f). The 3D view showed an active interaction of OVECs with the scaffold since the nuclei were placed along the collagen meshes in an organized manner (nuclei: blue; collagen meshes: green; Fig. 2e and Supplementary Video S3). It is worth mentioning that images were taken with the same 3D volume at both time points but at a different depth into the scaffold. This suggests that cells quickly enter the scaffold and then, possibly with an active movement, invade the scaffold more deeply by following the collagen meshes.

### 3.3. ADMs influence the expression of genes involved in the angiogenic process

To investigate whether culturing OVECs onto ADMs modulates gene expression levels of the main factors (Fig. 3a and b) and receptors (Fig. 3a–c) related to the angiogenic process, we performed RT-qPCR on cells grown onto bovine and porcine collagen or fibronectin as 2D culturing control. As shown in Fig. 3b and d, ADMs significantly upregulated the expression of several angiogenic factors, such as Vascular Endothelial Growth Factor-A (*VEGFA*), Placental Growth Factor (*PGF*), and Interleukin-8 (*IL8*). We failed to detect the expression of Angiopoietin-1 (*ANGPT-1*), another important factor linked to the angiogenic process. Conversely, the expression levels of angiogenic receptors (Fig. 3c), such as Kinase insert Domain Receptor (*KDR*), Fms Related Receptor Tyrosine Kinase 1 (*FLT1*), and TEK Receptor Tyrosine Kinase (*TEK*), were downregulated in OVECs grown onto the bovine and porcine collagen scaffolds. In addition, we investigated the expression levels of other genes involved in the angiogenic pathways (Fig. 3d). Matrix metalloproteinase-2 (*MMP2*) mRNA level was found to be downregulated in 3D-culture conditions, whereas the expression of Interleukin-6 (*IL6*) was slightly upregulated in 3D-culture conditions,

but the observed changes did not reach statistical significance. No expression or modulation of the expression levels was observed for matrix metalloproteinase-9 (*MMP9*), a gene involved in the remodeling of the ECM, Tumor Necrosis Factor- $\alpha$  (*TNF*), as an inflammation marker, and C-C Motif Chemokine Ligand 2 (*CCL2*), a factor involved in monocyte recruitment to sites of neo-angiogenesis (Supplementary Table S3).

In the angiogenic context, the microenvironment (*i.e.*, neighboring cells, soluble factors, physical fields, ECM) plays a pivotal role in influencing cell behavior [62]. In fact, several studies established that 3D culturing conditions can modulate the gene expression profile of factors involved in the angiogenic process [63–65]. As expected, OVECs cultured onto collagen scaffolds, both bovine and porcine, modified their gene expression profile by upregulating angiogenic factors (*VEGFA*, *PGF*, and *SEMA3A*). VEGF-A is the main angiogenic factor, and its expression is triggered by hypoglycemia and, most of all, by hypoxia [66,67], a condition that could manifest during our *in vitro* 3D culture, but also during the graft-related ischemic/hypoxic window. PGF is primarily expressed in placental tissue, and it has a role in trophoblast invasion into the maternal decidua [68]. Even though its role in physiological angiogenesis is clear (*i.e.*, stimulation of growth, migration, and survival of ECs, and vessel maturation), PGF expression under hypoxia is still debated [69]. SEMA3A has an important function in controlling the angiogenic process and is frequently downregulated during tumor development [70]. Its expression in our 3D culture indicates that the angiogenic process is physiologically regulated. On the contrary, the expression of all the angiogenic receptors (*KDR*, *FLT1*, *NRP1*, and *TEK*) was strongly downregulated. The expression levels of these receptors are not directly controlled by hypoxia [71]. This decreased expression could be part of a negative regulation loop, tightly orchestrating the angiogenic process.

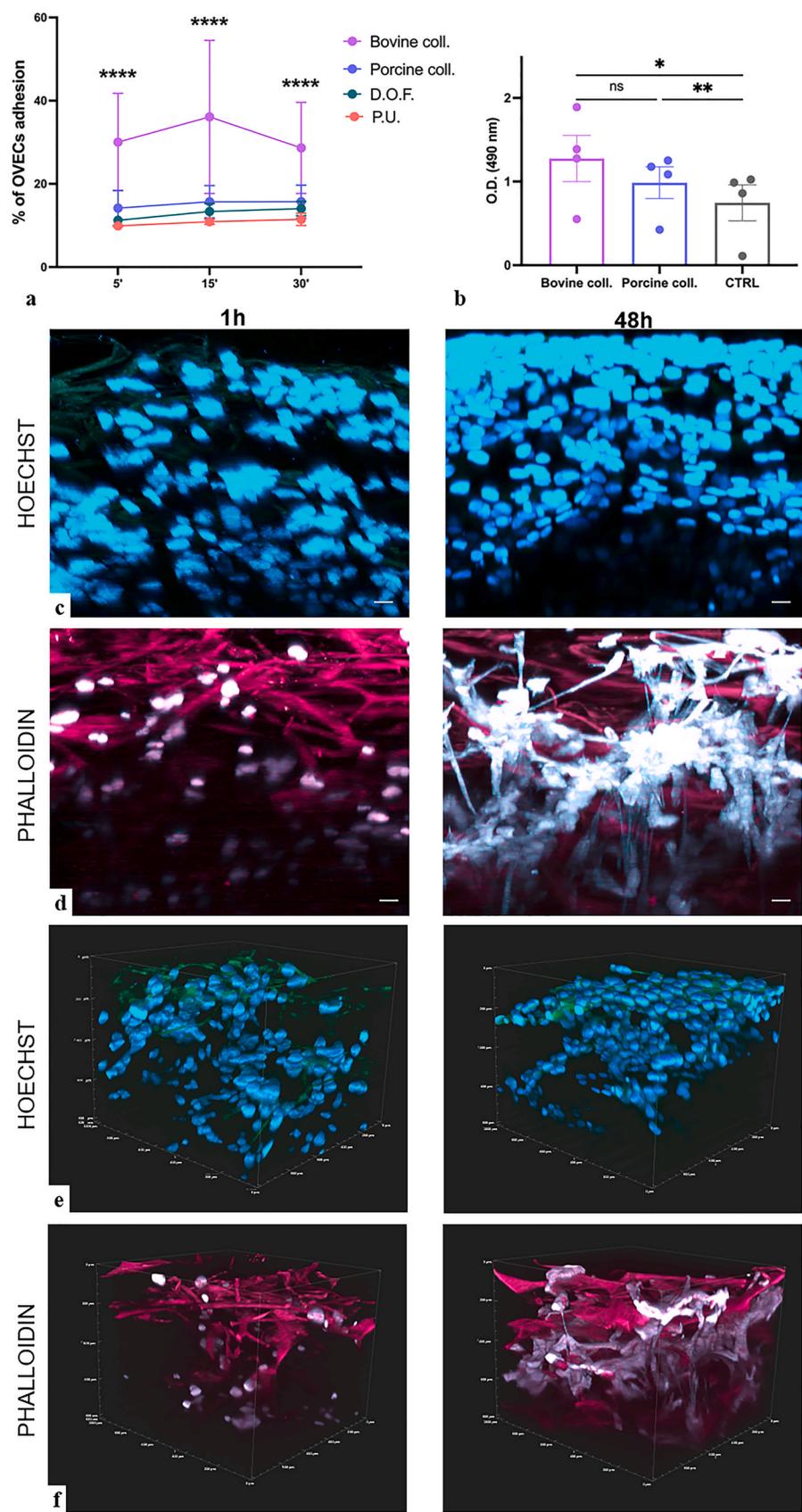
Since the remodeling of the ECM is one of the first steps occurring during the angiogenic process, the downregulation of *MMP2* in 3D-culture was unexpected. *MMP2* and *MMP9* are collectively known as gelatinases: *MMP2* can digest gelatin, type I, type IV, and type V collagens, vitronectin, and elastin, while *MMP9* cleaves type IV, type V, type VII, type X, and type XIV, but not type I collagens, laminin, and fibronectin [72]. Both MMPs play a crucial role during physiological angiogenesis, which occurs in placentation [73] and wound healing [74], while their overexpression is associated with tumor angiogenesis [75]. Thus, the downregulation of *MMP2* and the undetectable expression of *MMP9* suggest that our pre-seeded scaffolds may mimic a physiological state of controlled angiogenesis.

Taken together these data, we can assert that the bovine collagen scaffold is the most suitable ADM for translation into *in vivo* applications.

### 3.3. Animal model of ATMP transplantation and evaluation of revascularization and tissue viability

Follicular maturation in the pre-ovulatory phase lasts, on average, 14 days, and the growth of the dominant follicle is connected to its degree of vascularization. The ischemic/hypoxic window after OTT, lasting 7–10 days post-implantation, causes the loss of more than 60 % of follicles [2,76]. Thus, we employed a xenograft mouse model to understand whether graft supplementation with OVECs may represent a successful approach to improve the vascularization rate and post-grafting tissue survival.

After processing ovarian biopsies for the implantation procedure (Fig. 4a and Supplementary Fig. S6a), we aimed to characterize pre-implantation vascularization of ovarian tissue slices via human CD31/PECAM1 (hCD31) staining (Supplementary Fig. S6b). Then, tissue slices were subcutaneously transplanted into the backs of female NSG mice (Fig. 4a). After 14 days, grafts were excised and fixed, and Quantigene 2.0 Assay was performed to determine mRNA levels of AMH, a marker of ovarian reserve. Macroscopic evaluations of grafted tissues suggested that OVEC supplementation increased tissue revascularization (Fig. 4b and Supplementary Fig. S7). Moreover, evaluation of tissue architecture



(caption on next page)



**Fig. 2. Interaction between OVECs and different ADMs.** (a) The adhesion assay was performed by seeding FAST DiI-labeled OVECs onto the different ADMs for 5, 15, or 30 min. After removing non-adherent cells, OVECs were lysed to release the dye in solution, and the fluorescence was read. Results are expressed as percentage of cell adhesion with reference to a calibration curve established with an increasing number of labeled cells. Data are presented as mean  $\pm$  standard error mean (SEM) of independent experiments conducted in duplicate ( $n = 3$ ). \*\*\*\* $p < 0.0001$  (Two-way ANOVA). (b) The proliferation assay was conducted by seeding OVECs onto the scaffolds for 72 h. MTS was then added, and the absorbance was read at 490 nm by a plate reading spectrophotometer. Results are presented as the mean  $\pm$  SEM of independent experiments conducted in duplicate ( $n = 4$ ). Cells cultured onto fibronectin were used as control (CTRL). \* $p < 0.05$ ; \*\* $p < 0.01$  (one-way ANOVA). (c–f) Multiphoton microscopy imaging of OVECs seeded onto bovine collagen scaffold for 1 h or 48 h. Nuclei were stained with HOECHST (blue) (c). 48 h after the seeding, cells were more abundant compared to cells fixed after 1 h, indicating they proliferated. Phalloidin staining (light pink) (d) and 3D reconstruction (f) highlighted that OVECs after 48 h were more spread compared to the initial timing (1 h). Scale bars, 50  $\mu$ m. Bovine collagen scaffolds are represented in green (c) and bright pink (f). Representative images were taken with A1R MP confocal multiphoton microscope (Nikon).

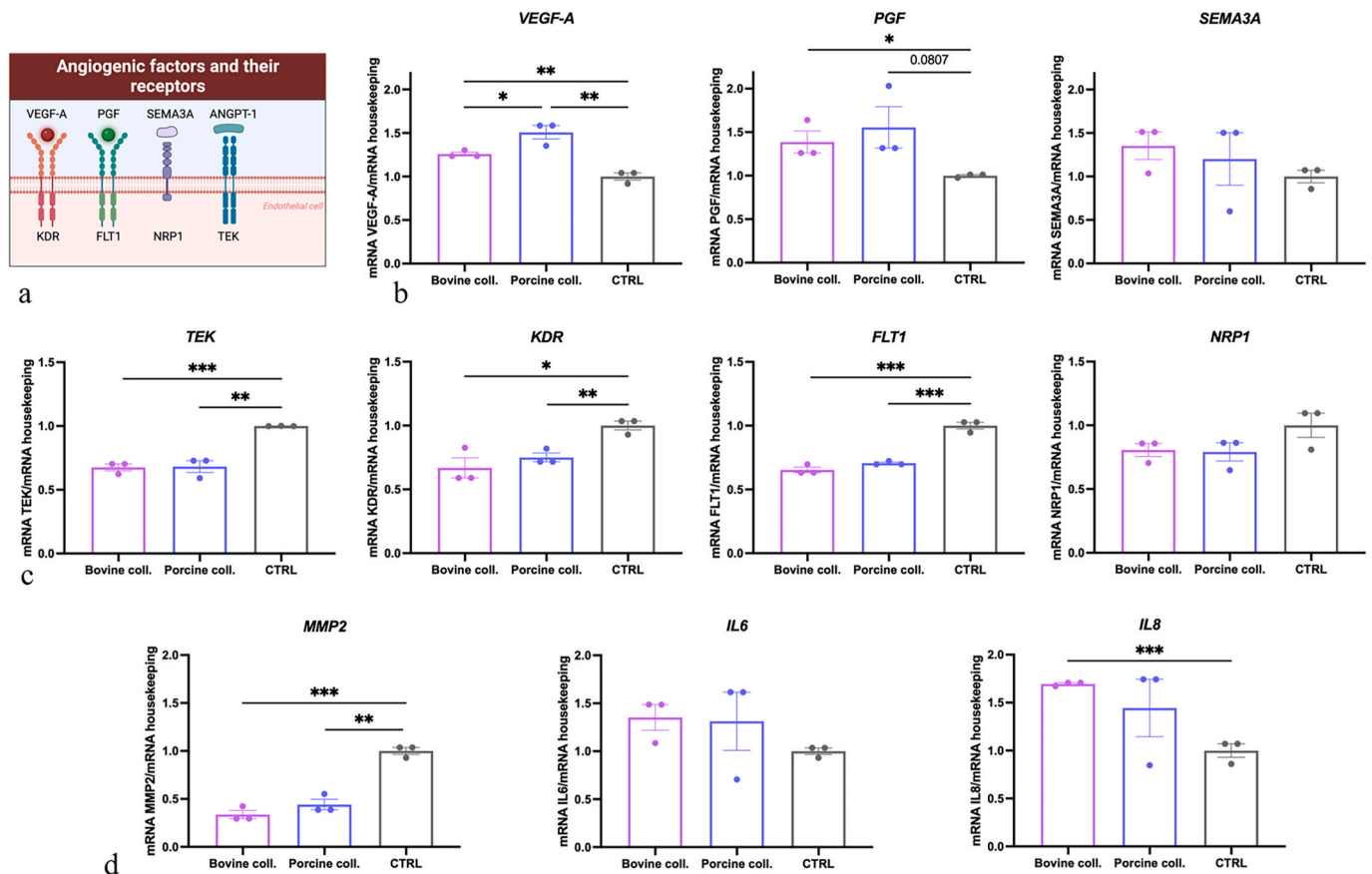


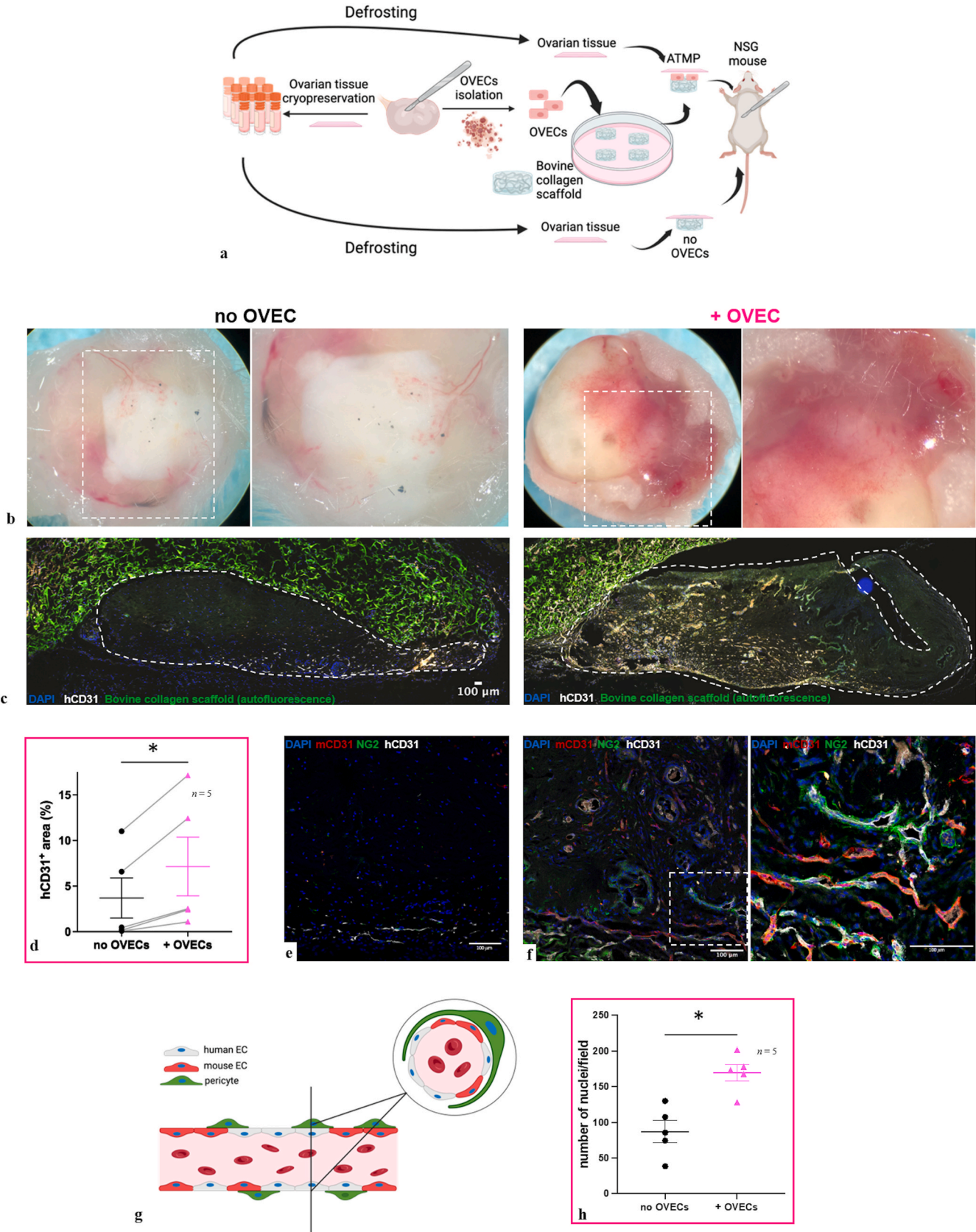
**Fig. 3. Gene expression modulation of the main factors involved in the angiogenic process.** (a) Schematic representation of angiogenic factors and their respective receptors. RT-qPCR of *VEGFA*, *PGF*, *SEMA3A* (b), *KDR*, *FLT1*, *NRP1*, *TEK* (c), *MMP2*, *IL6*, and *IL8* (d) expressed by OVECs seeded onto bovine or porcine collagen scaffolds, or fibronectin (CTRL) for 48 h. The gene expression levels are reported as fold of increase with respect to the mean of normalized values of *GAPDH* and *TBP* (housekeeping genes). Data are expressed as the mean  $\pm$  standard error mean of independent experiments conducted in duplicate ( $n = 3$ ). \* $p < 0.05$ ; \*\* $p < 0.01$ ; \*\*\* $p < 0.001$  (unpaired two-tailed *t*-test).

by hematoxylin-eosin (H&E) staining revealed a higher tissue cellularization in the presence of OVECs (Supplementary Fig. S6d). Graft revascularization was also assessed by performing IF for hCD31 (Fig. 4c): the percentage of the hCD31-positive area inside the ovarian tissue (dotted area) was statistically significantly higher in OVECs-supplemented graft compared to the tissue transplanted alone (Fig. 4d).

To better characterize the vasculature, post-grafting ovarian tissue sections were stained for NG2 as well, a perivascular cell marker [24]. Confocal microscopy images showed that OVECs-supplemented grafts presented numerous NG2-positive vessels (Supplementary Fig. S6c), highlighting the presence of mature and stable vasculature. The staining for hCD31 and mouse CD31 (mCD31) allowed the detection of numerous chimeric vessels (Fig. 4g) at the interface between OVECs-supplemented scaffolds and the ovarian tissue (Fig. 4f and Supplementary Fig. S6d) but not in the absence of OVECs (Fig. 4e). This result suggested the formation of a vascular network between

supplemented human OVECs and host ECs.

Furthermore, additional *in vivo* experiments were performed to evaluate the vasculature system at 30 days post-grafting procedure. Macroscopic evaluation of the excised transplants (Supplementary Fig. S8a) confirmed that the main differences were between OVECs-supplementation and without OVECs-supplementation, with no apparent alterations in the revascularization levels between 14 and 30 days. The results of the IF staining clearly support literature findings [24], as tissue vascularization levels in the subcutaneous transplant model decrease at 30 days compared to 14 days post-transplantation. Subcutaneous transplantation in the dorsal skin of mice is widely used to study revascularization during wound healing [77]. However, this model has also been employed in OTT research due to its favorable environment for follicular survival and the development of a rich neo-vascular network around the graft. This site also provides a larger manipulation and transplantation field [78]. Several studies have



(caption on next page)

**Fig. 4. Schematic visualization of the experimental design, macroscopic results, and histological evaluation.** (a) Ovarian biopsy was partly cut into tissue slices for vitrification and partly digested for OVEC isolation. OVECs were seeded onto the bovine collagen scaffold and transplanted in the back of female NSG mice. (b) After 14 days, the macroscopic evaluation of the excised grafts indicated a higher vascularization of the graft supplemented with OVECs compared to the tissue grafted alone. (c) IF for hCD31 (white) of excised graft with or without OVECs supplementation. Bovine collagen scaffold presents a characteristic autofluorescence in the green channel. Images were acquired using a Nikon Eclipse Ti-E inverted fluorescent microscope equipped with a DC-152Q-C00-FI and NIS V4.30 software (Nikon), as well as a ZEISS LSM 880 with Airyscan. Stitched images were acquired using NIS V4.30 software (Nikon). (d) Quantification of the area positive for hCD31 normalized on the area of human ovarian tissue (dotted area). Data are represented as the mean  $\pm$  standard error mean (SEM) of independent experiments ( $n = 5$ ). \* $p < 0.05$  (paired two-tailed  $t$ -test). (e, f **left panel**) IF staining of mouse CD31 (mCD31; red), human CD31 (hCD31; grey), and NG2 (green) showed that graft supplementation with OVECs resulted in the formation of mature vessels, stabilized by NG2-positive perivascular cells. (f **right panel**) Zoomed field of IF staining showing stabilized vessels. (e) On the contrary, no vascularization was observed in the absence of OVECs. At least four images were acquired per sample. Images were analyzed using ImageJ2 (Fiji) software. Z projection was performed on maximum intensity. (g) Schematic visualization of newly formed chimeric vessels. (h) Nuclei staining (blue) showed a significantly higher cellular density in ovarian tissue transplantation supported by OVECs supplementation. Data are represented as the mean  $\pm$  SEM of independent experiments ( $n = 5$ ). \* $p < 0.05$  (paired two-tailed  $t$ -test).

specifically investigated the revascularization process in OTT within the first two weeks post-transplantation, highlighting the crucial role of host-derived vascular ingrowth and angiogenic factors in facilitating neovascularization [20,79]. Beyond this initial phase, research has primarily focused on long-term graft viability and follicular survival, as sustained vascularization is essential for maintaining follicular function [80,81]. Comparative studies have also examined the differences between early and late-stage graft integration, emphasizing how prolonged ischemic stress and delayed revascularization can negatively affect follicular density and function.

Since tissue viability increases with cellularization, we assessed the number of nuclei inside the ovarian slices as markers of tissue viability. OVECs-supplementation significantly increased the number of nuclei/field compared to the tissue grafted alone (Fig. 4h).

Our results suggest that endothelial supplementation improves tissue viability, possibly favoring follicle viability as well. In fact, QuantiGene Assay showed that OVECs-supplementation increased the gene expression of *AMH* (Supplementary Fig. S9) in three samples out of four.

It is known that ECs can secrete essential ‘angiocrine factors’ and ovarian ECs promote early follicular development and survival [82]. Moreover, a positive correlation between vascularization and primordial follicle survival has been previously demonstrated, either through a pro-angiogenic approach [30], by functionalizing the scaffold with an angiogenic-stimulating factor, or through an inosculation approach [83], involving the pre-seeding of cells with pro-angiogenic capability. Regarding the first approach, Gao et al. [18], using a syngeneic mouse model of OTT, demonstrated that modifying hydrogels with bFGF significantly increased PMF survival, proliferation, and vessel density (IHC for CD31) at seven days post-transplantation, while reducing apoptosis. A strong positive correlation between microvascular density and PMF count confirmed the role of bFGF-induced neoangiogenesis in follicle preservation. Mannavella et al. [84] seeded ADSCs onto a fibrin scaffold during the OTT. On day 7 post-transplantation, the total vessel area, assessed by CD34<sup>+</sup> staining, was significantly greater in the group treated with the ADSC-loaded scaffold; the survival rate of PMFs was also higher. Finally, a significant positive correlation was established between follicle survival rates and the total CD34<sup>+</sup> endothelial area.

Over recent years, several research groups have attempted to increase graft revascularization with different strategies. Previous evidence has already demonstrated the capability of bovine collagen scaffolds to stimulate tissue revascularization under hypoxic conditions [24,43]. Moreover, the use of scaffolds appeared as a promising approach to also support follicle growth to develop an “artificial ovary”. As indicated by Fazelian-Dehkordi et al., decellularized sheep omentum actively supported the *in vitro* maturation of follicles, probably due to the presence of growth factors and proteins inside the scaffold [85]. Similar findings suggest that the microenvironment plays a central role in the success of the OTT procedure [86]. Abir et al. demonstrated that using collagen scaffolds to support OTT resulted in improved revascularization, a greater number of recovered follicles, fewer atretic follicles, increased Ki67<sup>+</sup> granulosa cells, and a decreased presence of apoptotic stromal cells [87].

Another strategy to ameliorate ovarian tissue engraftment consisted of the co-transplantation of stem cells during OTT. MSCs and ADSCs are widely used in regenerative medicine [88,89]. In the context of OTT, the use of MSCs or ADSCs has raised accumulating interest due to their capability of increasing vascularization and tissue survival [25,90–92]. Ma et al. demonstrated that pre-treating the ovarian tissue with Follicle Stimulating Hormone (FSH) prior to transplantation increased VEGF-A expression, thereby accelerating post-grafting revascularization [93]. The simultaneous treatment with VEGF-A and bFGF ameliorated tissue survival [94] and improved tissue vascularization [95]. Several studies have proposed combined strategies with encouraging outcomes, such as VEGF-165 supplementation in concert with the usage of collagen scaffolds [96] or the application of ADSC-pre-seeded collagen scaffolds [97].

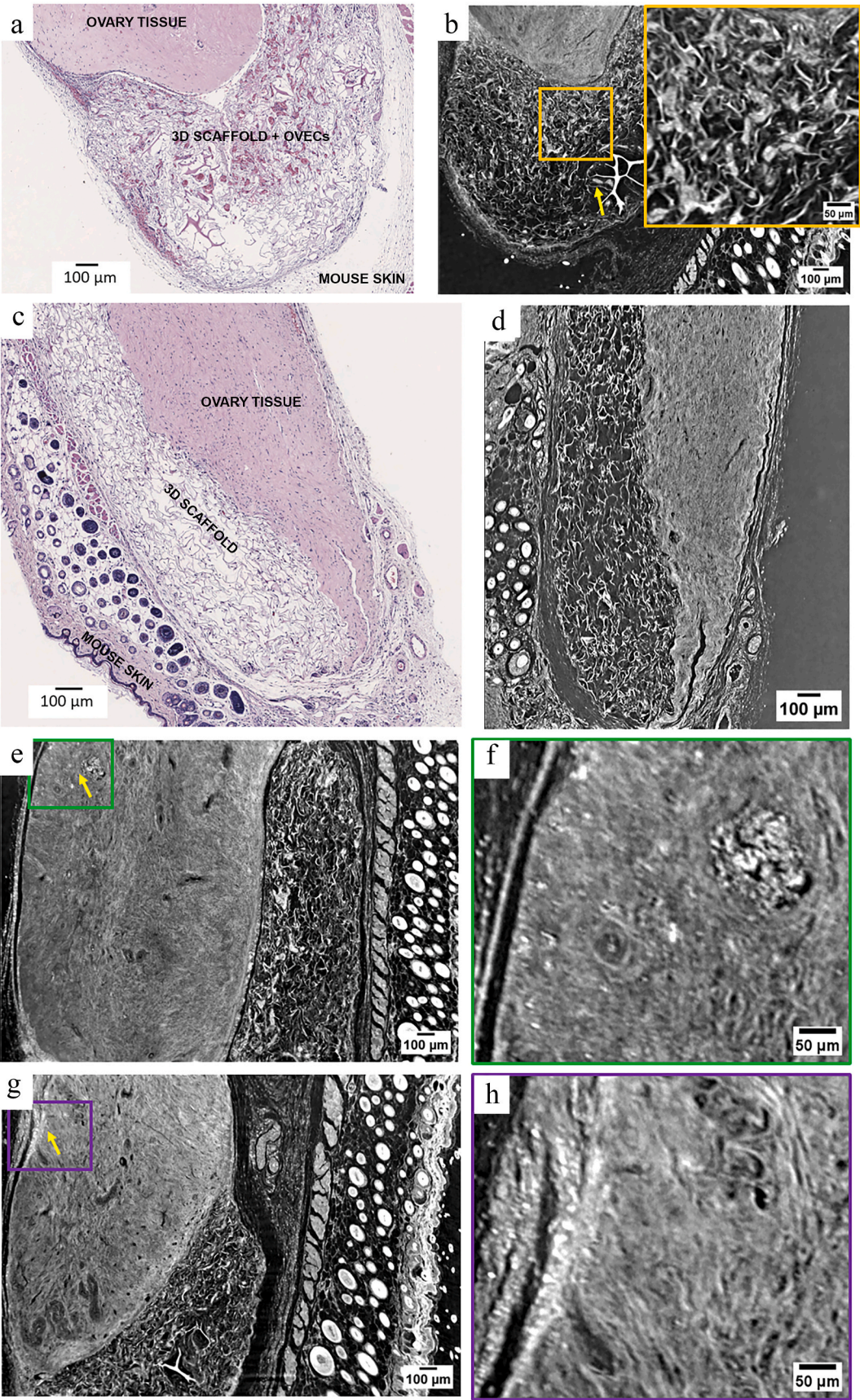
Our contribution to the field perfectly fits into this scientific background, suggesting that the combination of ECs and ATMPs may be a winning strategy to improve OTT. In fact, our animal model allowed us to confirm the hypothesis that ECs supplementation onto bovine collagen scaffolds could significantly increase post-grafting revascularization.

### 3.5. Observation of tissue revascularization by X-ray phase-contrast microtomography

We thus proceeded with a more in-depth analysis of tissue revascularization by synchrotron radiation-based phase-contrast microtomography (microCT), a technique known in the literature also as virtual histology [98]. This approach is a non-invasive, high-resolution, multi-scale 3D imaging method, well suited for retrieving structural and anatomical information of biological specimens, especially tissues [99–102], due to the peculiar advantages provided by phase-contrast [103,104].

Fig. 5a displays a representative H&E staining of a grafted tissue by optical microscopy, where the OVECs-supplementation is clearly visualized in the bovine collagen matrix. Strikingly, the histological examination reveals a significant presence of OVECs within the matrix organized to form vascular structures (red) whose functionality is demonstrated by the presence of red blood cells inside the vessels. Fig. 5b shows reconstructed virtual slices from X-ray phase-contrast microCT. In detail, the images depict a cropped area at the interface between the bovine collagen matrix and grafted human ovarian tissue, similarly to the region of interest displayed by histology in Fig. 5a. In accordance with the histological representation, X-ray images show aggregates of dense material within the scaffold matrix (Fig. 5b). These large light grey dots (pointed by yellow arrow) might be attributable to the massive presence of supplemented OVECs, organized in vessel-similar structures, as they appear denser than the surrounding matrix, possibly due to a locally high concentration of red blood cells. Their distribution can be even followed within the acquired volume (see Supplementary Video S4). The inset in Fig. 5b shows a potential accumulation of OVECs within the scaffold at higher magnification. For comparison, an unstained human ovarian tissue was imaged as well, and grafted within a bovine collagen matrix, without OVECs, by H&E





(caption on next page)



**Fig. 5. X-ray phase-contrast microCT examination of excised ovarian grafts.** (a) Region of interest of a H&E slice showing OVECs forming perfused vessels, as they are filled with red blood cells (red dots), within the bovine scaffold matrix in the OVECs-supplemented tissue subjected to X-ray phase-contrast microCT examination. (b) X-ray phase-contrast microCT virtual slice of the paraffin-embedded OVECs-supplemented tissue. Yellow arrow points to dense structures within the bovine scaffold, representing clusters of OVECs, as confirmed by the histological image. Zoomed view of the area highlighted with higher magnification the dense structures detected within the bovine scaffold. (c) H&E slice of ovarian tissue grafted without OVECs-supplementation. (d) X-ray phase contrast microtomography virtual slice of the same sample. (e–h) X-ray phase-contrast microtomography virtual slices of the OVECs-supplemented tissue, selected at different depths within the acquired volume. Yellow arrows point out very dense structures, as a likely accumulation of OVECs. (f) High magnification visualization of the dense structures detected and highlighted by the green rectangle in (e). (h) Zoomed inset depicting the distribution of OVECs visible within the violet rectangle drawn in (g).

(Fig. 5c) and by X-ray phase-contrast microCT (Fig. 5d). Unlike Fig. 5a, the histology of this control specimen confirms the lack of exogenous ECs both in the ovarian tissue and scaffold spaces (Fig. 5c). In Fig. 5d, X-ray phase-contrast microCT shows an empty scaffold and the absence of dense structures in the ovarian tissue morphology (see [Supplementary Video S5](#)). Phase-contrast microCT examination was also exploited to visualize the ovary vasculature. For the first time, it has been demonstrated by ex vivo analysis (IHC) that the bovine collagen 3D scaffold (Integra®), supplemented with human ECs can induce the formation of a vascular bed inside the matrix itself, with an evident new blood supply (red blood cell presence).

Fig. 5e and g display an overview of other reconstructed virtual planes of the OVECs-supplemented tissue, selected at different depths in the reconstructed volume. Endogenous vessels were clearly

distinguished within the tissue with a contrast resolution capable of also discriminating the inner vessel walls. In addition, we detected the presence of dense white spots along one side of the ovarian tissue (yellow arrows; Fig. 5e–g) and at the lower border with the bovine collagen matrix. Zoomed views of the areas marked with colored rectangles are displayed in Fig. 5f and h. Likely, the intense signal is caused by an accumulation of red blood cells in the ovarian tissue, which may have occurred after an ECs migration through the matrix. This evidence suggests a potentially preferential side for OVECs accumulation and formation of new vessels in the ovarian tissue.

In addition to a clear visualization of the vascular system, comprising both endogenous and newly formed vessels, the tomographic reconstruction highlighted a well-preserved state of the ovarian tissue following cryopreservation and subsequent transplantation. Fig. 6a

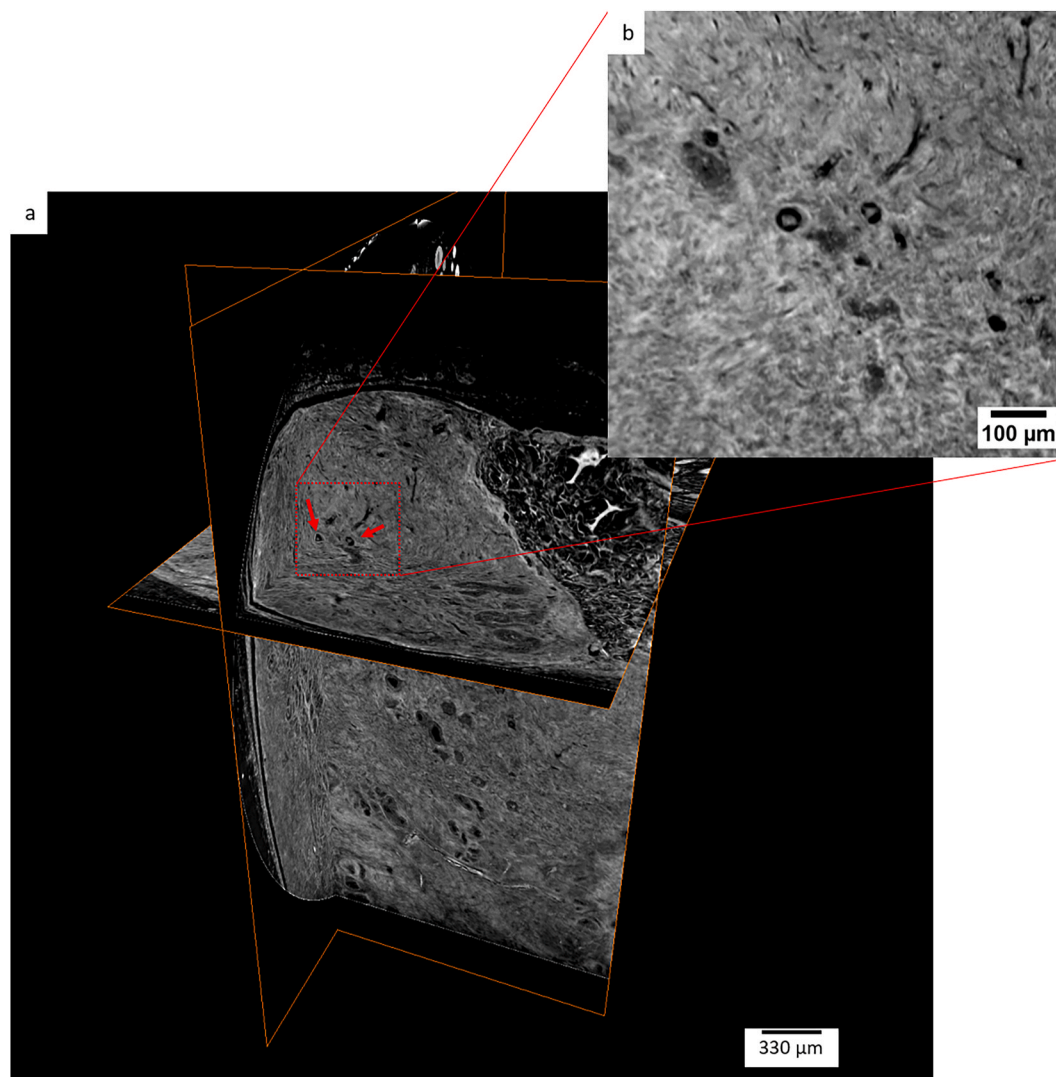


**Fig. 6. Representations of arbitrary orthogonal planes within the imaged OVECs supplemented tissue.** (a) Red arrows point out healthy follicles within a well-preserved tissue. (b) Zoomed image of the two follicles.



shows a representation of the OVECs-supplemented tissue by arbitrary crossing orthogonal slices. Red arrows indicate the presence of two spherical structures (Fig. 6b) with a measured diameter of 44.5  $\mu\text{m}$  and 32.5  $\mu\text{m}$ , respectively, compatible with healthy primary or primordial follicles within the tissue [105].

X-ray phase-contrast microCT was used to image grafted OVECs-supplemented ovarian tissue after staining with iodine. Iodine contrast agent has been previously demonstrated to be effective for enhancing cellular visualization in X-ray imaging applications [54]. Fig. 7 shows a series of maximum-intensity projection images, emphasizing at the same

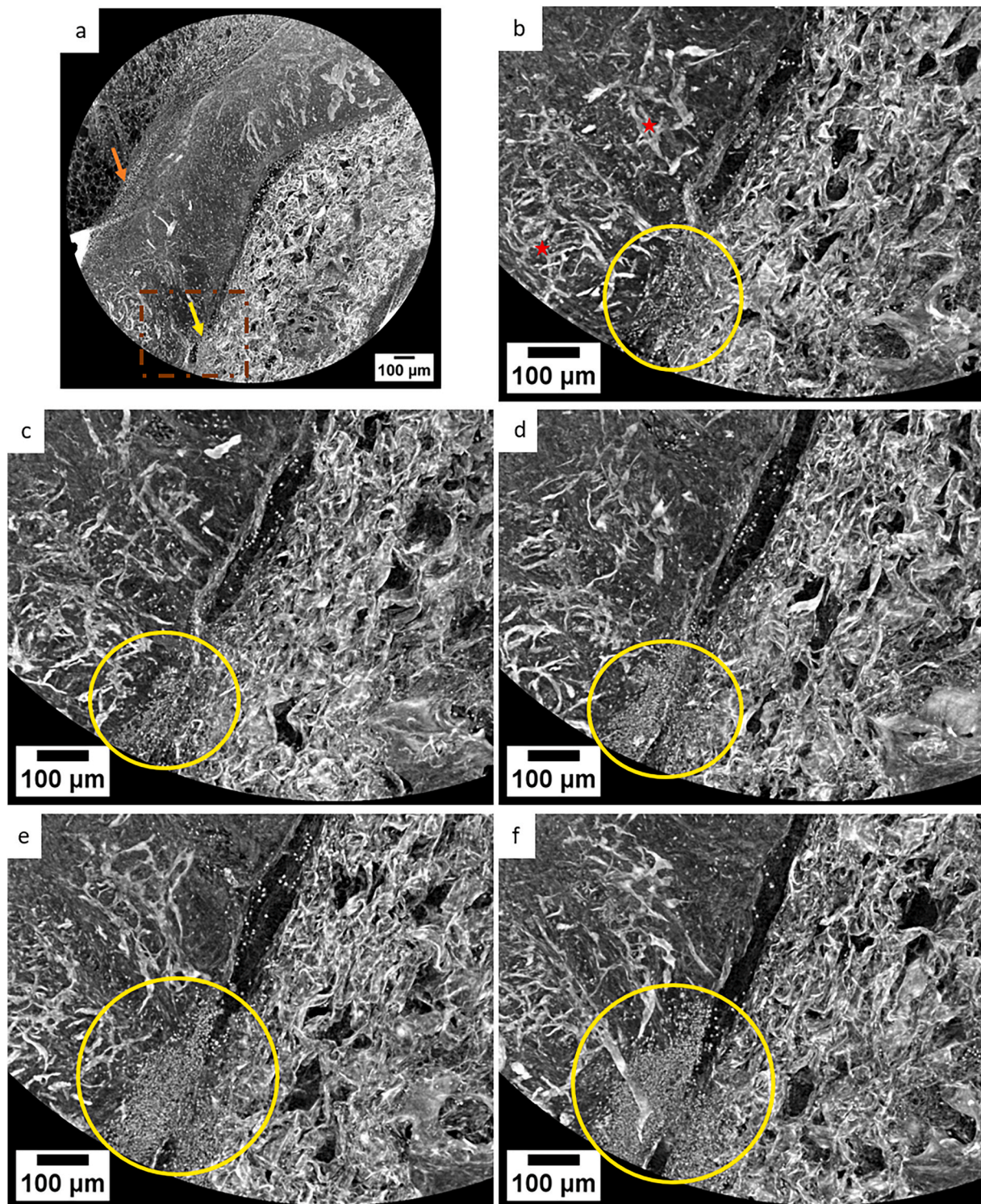


**Fig. 7.** Representations of the imaged OVECs supplemented tissue stained with iodine. (a) OVECs-supplemented iodine-stained tissue virtual section obtained by maximum intensity projection of selected X-ray phase-contrast microtomography slices. The human ovarian tissue is visible next to the bovine collagen scaffold. This visualization highlights the vascular system within the ovarian tissue and ECs accumulation on a preferential side (orange arrow) and EC migration from the scaffold to the tissue (yellow arrows). (b–f) Sequential sections (extracted from the sub-area displayed in the panel a with a brown dashed line) showing the gradual invasion of the OVECs at different depths within the imaged whole sample.



time the endogenous vascular network with large vessels visible in the middle of the ovarian tissue and the accumulation of new ECs (bright spots pointed by orange and yellow arrows). Specifically, yellow arrows indicate cell migration from bovine collagen scaffold to ovarian tissue at different depths within the imaged volume (see [Supplementary Video S6](#)).

#### 4. Conclusions

The ischemic/hypoxic window following OTT is the primary cause of follicle loss. In this study, we successfully demonstrated that supplementing OTT with OVECs doubled the revascularized area compared to the tissue transplanted alone. Additionally, preliminary evidence of improved follicular survival, indicated by increased AMH expression level, suggested enhanced ovarian function.

One potential limitation of this approach is the need to sacrifice part of the ovarian biopsy to isolate OVECs, raising ethical consensus regarding the reduction of tissue available for cryopreservation. To address this point, we propose to isolate OVECs from the medullary part rather than cortical ovary tissue or minimize the size of the starting tissue by expanding OVECs in a bioreactor. Additionally, ECs from alternative body areas, such as skin biopsies, or the use of a pro-angiogenic cell mixture, the SVF, isolated from lipoaspirate through a minimally invasive procedure, could serve as suitable substitutes. A hybrid strategy, combining automated cell isolation with cGMP-grade bioreactor expansion, may further enhance the feasibility of this approach for clinical translation.

As a next step, we aim to set up a cGMP-grade xeno-free protocol for EC isolation and expansion, ensuring compliance with cell therapy standards. *In vivo* validation will be performed by using ovariectomized murine models that, after the human OTT, will be stimulated with human FSH to assess follicular response and evaluate circulating markers of ovarian reserve (AMH or estrogens).

A key goal of this research was to try to bridge the gap between experimental and clinical applications. Using a clinically approved matrix, already recognized as the gold standard for non-healing wounds, could reduce the timing of regulatory approval, positioning this approach as a potential “drug repurposing” strategy. Indeed, this study has the potential to pave the way for utilizing this scaffold in other tissue contexts and for novel applications. We are confident that the repositioning of a 3D matrix can have a profound impact, particularly now that the OTT has been “promoted” by the American Society for Reproductive Medicine (ASRM) from “experimental procedure” to “clinical practice”.

From a biomaterials perspective, our study pioneered innovative approaches to investigate biocompatibility and cellular colonization of 3D scaffolds, employing X-ray phase-contrast microtomography and multi-photon microscopy. For the first time, *ex vivo* IHC analysis demonstrated that a bovine collagen 3D scaffold, supplemented with human ECs, is able to induce the formation of a vascular bed within the matrix itself, accompanying an evident new blood supply.

In conclusion, we have successfully established a method for the isolation and extensive characterization of OVECs. Adhesion and proliferation assays indicated the bovine collagen scaffold as the most promising for seeding OVECs and testing transplantation in the animal model. Our results clearly demonstrated that using OVECs during the ovarian tissue transplantation procedure resulted in an improved vascularization of the grafted tissue and an increased AMH expression.

#### CRediT authorship contribution statement

**Mariagiulia Spazzapan:** Writing – review & editing, Writing – original draft, Visualization, Validation, Software, Methodology, Investigation, Formal analysis, Data curation, Conceptualization. **Silvia Pegoraro:** Writing – review & editing, Methodology, Investigation, Data curation. **Roman Vuerich:** Validation, Methodology, Investigation, Conceptualization. **Gabriella Zito:** Resources, Formal analysis, Data

curation. **Andrea Balducci:** Writing – review & editing, Writing – original draft, Formal analysis. **Elena Longo:** Writing – review & editing, Visualization, Methodology. **Lorella Pascolo:** Writing – original draft, Supervision, Software, Conceptualization. **Miriam Toffoli:** Methodology, Investigation, Data curation. **Giorgia Meshini:** Writing – review & editing, Visualization, Methodology, Data curation. **Alessandro Mangogna:** Writing – original draft, Formal analysis, Data curation. **Gloria Ros:** Writing – review & editing, Visualization. **Francesca Buonomo:** Visualization, Formal analysis. **Federico Romano:** Resources. **Letizia Lombardelli:** Methodology. **Giovanni Papa:** Validation, Resources. **Marie-Pierre Piccinni:** Writing – review & editing, Funding acquisition. **Serena Zacchigna:** Writing – review & editing, Supervision, Resources, Funding acquisition. **Chiara Agostinis:** Writing – review & editing, Writing – original draft, Project administration, Investigation, Formal analysis, Data curation, Conceptualization. **Roberta Bulla:** Writing – review & editing, Supervision, Resources, Funding acquisition, Conceptualization. **Giuseppe Ricci:** Writing – review & editing, Funding acquisition, Formal analysis, Conceptualization.

#### Ethics approval and consent to participate

The study was reviewed and approved by the Regional Ethical Committee of FVG (CEUR, Udine, Italy; prot. 0010143/P/GEN/ARCS 2019).

All animal procedures were performed according to the protocol EU Directive 2010/63/EU, approved by the ICGEB Animal Welfare Board and by the Italian Ministry of Health.

#### Funding

This work was supported by the Ministry of Health, Rome - Italy, in collaboration with the Institute for Maternal and Child Health IRCCS Burlo Garofolo, Trieste – Italy (RC23/18 and RC20/23 to G.R.), by the National Recovery and Resilience Plan (NRRP), funded by the European Union - Next Generation EU (CUP J53D23001020006 to R.B.), and by PON Research and Innovation Program (REACT EU 2014-2020) for the financial support provided to M.S.'s PhD.

#### Declaration of competing interest

The authors declare no competing interests.

#### Acknowledgements

We thank Gabriele Baj and CIMA for their technical support, and Martina Palmieri for her help with patient enrollment. We acknowledge CERIC-ERIC (granted proposal 20237180) and Euro-BioImaging ([www.eurobioimaging.eu](http://www.eurobioimaging.eu)) for providing access to Elettra Sincrotrone Trieste.

#### Appendix A. Supplementary data

Supplementary data to this article can be found online at <https://doi.org/10.1016/j.bioactmat.2025.03.021>.

#### References

- [1] C. Ladanyi, A. Mor, M.S. Christianson, N. Dhillon, J.H. Segars, Recent advances in the field of ovarian tissue cryopreservation and opportunities for research, *J. Assist. Reprod. Genet.* 34 (2017) 709–722.
- [2] M.M. Dolmans, J. Donnez, L. Cacciottola, Fertility preservation: the challenge of freezing and transplanting ovarian tissue, *Trends Mol. Med.* 27 (2020) 777–791.
- [3] L. Cacciottola, J. Donnez, M.M. Dolmans, Ovarian tissue and oocyte cryopreservation prior to iatrogenic premature ovarian insufficiency, *Best Pract. Res. Clin. Obstet. Gynaecol.* 81 (2022) 119–133.
- [4] S.R. Mishra, H.F. Chung, M. Waller, G.D. Mishra, Duration of estrogen exposure during reproductive years, age at menarche and age at menopause, and risk of cardiovascular disease events, all-cause and cardiovascular mortality: a systematic review and meta-analysis, *BJOG* 128 (2021) 809–821.

- [5] L.M. Ataman, M.M. Laronda, M. Gowett, K. Trotter, H. Anvari, F. Fei, et al., A synopsis of global frontiers in fertility preservation, *J. Assist. Reprod. Genet.* 39 (2022) 1693–1712.
- [6] E.G.G. Preservation, R.A. Anderson, F. Amant, D. Braat, A. D'Angelo, S.M. Chuva de Sousa Lopes, et al., ESHRE guideline: female fertility preservation, *Hum. Reprod. Open* 2020 (2020) hoaa052.
- [7] Practice Committee of the American Society for Reproductive Medicine, Electronic address aao. Fertility preservation in patients undergoing gonadotoxic therapy or gonadectomy: a committee opinion, *Fertil. Steril.* 112 (2019) 1022–1033.
- [8] M.M. Dolmans, C. Hossay, T.Y.T. Nguyen, C. Poirot, Fertility preservation: how to preserve ovarian function in children, adolescents and adults, *J. Clin. Med.* 10 (2021).
- [9] M.M. Dolmans, J. Donnez, Fertility preservation in women for medical and social reasons: oocytes vs ovarian tissue, *Best Pract. Res. Clin. Obstet. Gynaecol.* 70 (2021) 63–80.
- [10] J. Donnez, M.M. Dolmans, D. Demylle, P. Jadoul, C. Pirard, J. Squifflet, et al., Livebirth after orthotopic transplantation of cryopreserved ovarian tissue, *Lancet* 364 (2004) 1405–1410.
- [11] M.M. Dolmans, T. Falcone, P. Patrizio, Importance of patient selection to analyze in vitro fertilization outcome with transplanted cryopreserved ovarian tissue, *Fertil. Steril.* 114 (2020) 279–280.
- [12] M. Izadpanah, R. Rahbarghazi, A.M. Seghinsara, A. Abedelahi, Novel approaches used in ovarian tissue transplantation for fertility preservation: focus on tissue engineering approaches and angiogenesis capacity, *Reprod. Sci.* 30 (2023) 1082–1093.
- [13] M.M. Dolmans, D.D. Manavella, Recent advances in fertility preservation, *J. Obstet. Gynaecol. Res.* 45 (2018) 266–279.
- [14] E. Dimitrova, L.A. Caromile, R. Laubenbacher, L.H. Shapiro, The innate immune response to ischemic injury: a multiscale modeling perspective, *BMC Syst. Biol.* 12 (2018) 50.
- [15] L. Cacciottola, J. Donnez, M.M. Dolmans, Ovarian tissue damage after grafting: systematic review of strategies to improve follicle outcomes, *Reprod. Biomed. Online* 43 (2021) 351–369.
- [16] X. Liu, K. Wu, L. Gao, L. Wang, X. Shi, Biomaterial strategies for the application of reproductive tissue engineering, *Bioact. Mater.* 14 (2022) 86–96.
- [17] A. Shikanov, Z. Zhang, M. Xu, R.M. Smith, A. Rajan, T.K. Woodruff, et al., Fibrin encapsulation and vascular endothelial growth factor delivery promotes ovarian graft survival in mice, *Tissue Eng. Part A* 17 (2011) 3095–3104.
- [18] J.M. Gao, J. Yan, R. Li, M. Li, L.Y. Yan, T.R. Wang, et al., Improvement in the quality of heterotopic allotransplanted mouse ovarian tissues with basic fibroblast growth factor and fibrin hydrogel, *Hum. Reprod.* 28 (2013) 2784–2793.
- [19] Y. Wang, Q. Chang, J. Sun, L. Dang, W. Ma, C. Hei, et al., Effects of HMG on revascularization and follicular survival in heterotopic autotransplants of mouse ovarian tissue, *Reprod. Biomed. Online* 24 (2012) 646–653.
- [20] L. Man, L. Park, R. Bodine, M. Ginsberg, N. Zaninovic, O.A. Man, et al., Engineered endothelium provides angiogenic and paracrine stimulus to grafted human ovarian tissue, *Sci. Rep.* 7 (2017) 8203.
- [21] D. Nugent, H. Newton, L. Gallivan, R.G. Gosden, Protective effect of vitamin E on ischaemia-reperfusion injury in ovarian grafts, *J. Reprod. Fertil.* 114 (1998) 341–346.
- [22] H.O. Olesen, S.E. Pors, L.B. Jensen, A.P. Gronning, C.E. Lemser, M.T.H. Nguyen Heimbürger, et al., N-acetylcysteine protects ovarian follicles from ischemia-reperfusion injury in xenotransplanted human ovarian tissue, *Hum. Reprod.* 36 (2021) 429–443.
- [23] J.S. Heo, S. Kim, Human adipose mesenchymal stem cells modulate inflammation and angiogenesis through exosomes, *Sci. Rep.* 12 (2022) 2776.
- [24] R. Vuerich, E. Groppa, S. Vodret, N.A.R. Ring, C. Stocco, F. Bossi, et al., Ischemic wound revascularization by the stromal vascular fraction relies on host-donor hybrid vessels, *NPJ Regen. Med.* 8 (2023) 8.
- [25] D.D. Manavella, L. Cacciottola, C.M. Desmet, B.F. Jordan, J. Donnez, C. A. Amorim, et al., Adipose tissue-derived stem cells in a fibrin implant enhance neovascularization in a peritoneal grafting site: a potential way to improve ovarian tissue transplantation, *Hum. Reprod.* 33 (2018) 270–279.
- [26] T. Liu, Y. Huang, L. Guo, W. Cheng, G. Zou, CD44+/CD105+ human amniotic fluid mesenchymal stem cells survive and proliferate in the ovary long-term in a mouse model of chemotherapy-induced premature ovarian failure, *Int. J. Med. Sci.* 9 (2012) 592–602.
- [27] Y. Zhou, J. Zhou, X. Xu, F. Du, M. Nie, L. Hu, et al., Matrigel/umbilical cord-derived mesenchymal stem cells promote granulosa cell proliferation and ovarian vascularization in a mouse model of premature ovarian failure, *Stem Cell. Dev.* 30 (2021) 782–796.
- [28] S. Herraiz, A. Buigues, C. Diaz-Garcia, M. Romeu, S. Martinez, I. Gomez-Segui, et al., Fertility rescue and ovarian follicle growth promotion by bone marrow stem cell infusion, *Fertil. Steril.* 109 (2018) 908–918, e2.
- [29] D. Lai, F. Wang, Z. Dong, Q. Zhang, Skin-derived mesenchymal stem cells help restore function to ovaries in a premature ovarian failure mouse model, *PLoS One* 9 (2014) e98749.
- [30] M.W. Laschke, M.D. Menger, Prevascularization in tissue engineering: current concepts and future directions, *Biotechnol. Adv.* 34 (2016) 112–121.
- [31] E.S. Gargus, H.B. Rogers, K.E. McKinnon, M.E. Edmonds, T.K. Woodruff, Engineered reproductive tissues, *Nat. Biomed. Eng.* 4 (2020) 381–393.
- [32] A. Dadashzadeh, S. Moghasssemi, A. Shavandi, C.A. Amorim, A review on biomaterials for ovarian tissue engineering, *Acta Biomater.* 135 (2021) 48–63.
- [33] K. Oktay, G. Bedoschi, F. Pacheco, V. Turan, V. Emirdar, First pregnancies, live birth, and in vitro fertilization outcomes after transplantation of frozen-banked ovarian tissue with a human extracellular matrix scaffold using robot-assisted minimally invasive surgery, *Am. J. Obstet. Gynecol.* 214 (2016), 94 e1–9.
- [34] T. Biswal, Biopolymers for tissue engineering applications: a review, *Mater. Today Proc.* 41 (2021) 397–402.
- [35] V.C. van der Veen, M.B. van der Wal, M.C. van Leeuwen, M.M. Ulrich, E. Middelkoop, Biological background of dermal substitutes, *Burns* 36 (2010) 305–321.
- [36] M. Piejko, K. Radziun, S. Bobis-Wozowicz, A. Waligorska, E. Zimolag, M. Nessler, et al., Adipose-derived stromal cells seeded on Integra(R) dermal regeneration template improve post-burn wound reconstruction, *Bioengineering (Basel)* 7 (2020).
- [37] A.C. Wosgrau, S. Jeremias Tda, D.F. Leonardi, M.J. Pereima, G. Di Giunta, A. G. Trentin, Comparative experimental study of wound healing in mice: pelnac versus Integra, *PLoS One* 10 (2015) e0120322.
- [38] S. Suzuki, K. Kawai, F. Ashoori, N. Morimoto, Y. Nishimura, Y. Ikada, Long-term follow-up study of artificial dermis composed of outer silicone layer and inner collagen sponge, *Br. J. Plast. Surg.* 53 (2000) 659–666.
- [39] S. Lun, S.M. Irvine, K.D. Johnson, N.J. Fisher, E.W. Floden, L. Negron, et al., A functional extracellular matrix biomaterial derived from ovine forestomach, *Biomaterials* 31 (2010) 4517–4529.
- [40] M.J. Smith, S.G. Dempsey, R.W. Veale, C.G. Duston-Fursman, C.A.F. Rayner, C. Javanapong, et al., Further structural characterization of ovine forestomach matrix and multi-layered extracellular matrix composites for soft tissue repair, *J. Biomater. Appl.* 36 (2022) 996–1010.
- [41] T. Kidd, V. Kolaityte, K. Bajaj, D. Wallace, D. Izadi, J. Bechar, The use of NovoSorb biodegradable temporising matrix in wound management: a literature review and case series, *J. Wound Care* 32 (2023) 470–478.
- [42] F.A. Auger, L. Gibot, D. Lacroix, The pivotal role of vascularization in tissue engineering, *Annu. Rev. Biomed. Eng.* 15 (2013) 177–200.
- [43] C. Agostinis, M. Spazzapan, R. Vuerich, A. Balducci, C. Stocco, A. Mangogna, et al., Differential capability of clinically employed dermal regeneration scaffolds to support vascularization for tissue bioengineering, *Biomedicines* 9 (2021).
- [44] G. Papa, M. Pangos, N. Renzi, V. Ramella, N. Panizzo, Z.M. Arnez, Five years of experience using a dermal substitute: indications, histologic studies, and first results using a new single-layer tool, *Dermatol. Surg.* 37 (2011) 1631–1637.
- [45] P. Taupin, A. Gandhi, S. Saini, Integra(R) dermal regeneration template: from design to clinical use, *Cureus* 15 (2023) e38608.
- [46] N.O. Ojeh, J.D. Frame, H.A. Navsaria, In vitro characterization of an artificial dermal scaffold, *Tissue Eng.* 7 (2001) 457–472.
- [47] S.G. Dempsey, C.H. Miller, J. Schueler, R.W.F. Veale, D.J. Day, B.C.H. May, A novel chemotactic factor derived from the extracellular matrix protein decorin recruits mesenchymal stromal cells in vitro and in vivo, *PLoS One* 15 (2020) e0235784.
- [48] A. Li, B.L. Dearman, K.E. Crompton, T.G. Moore, J.E. Greenwood, Evaluation of a novel biodegradable polymer for the generation of a dermal matrix, *J. Burn Care Res.* 30 (2009) 717–728.
- [49] C. Agostinis, E. Masat, F. Bossi, G. Ricci, R. Menegazzi, L. Lombardelli, et al., Transcriptomics and immunological analyses reveal a pro-angiogenic and anti-inflammatory phenotype for decidual endothelial cells, *Int. J. Mol. Sci.* 20 (2019).
- [50] R.D. McCurdy, J.J. McGrath, A. M-S. Validation of the comparative quantification method of real-time PCR analysis and a cautionary tale of housekeeping gene selection, *Gene Ther. Mol. Biol.* 12 (1) (2008) 1215–1224.
- [51] M.P. Piccinni, L. Lombardelli, F. Logiodice, D. Tesi, O. Kullolli, R. Biagiotti, et al., Potential pathogenetic role of Th17, Th0, and Th2 cells in erosive and reticular oral lichen planus, *Oral Dis.* 20 (2014) 212–218.
- [52] L. Lombardelli, F. Logiodice, M.P. Piccinni, Evaluation of gene expression profiling by QuantiGene 2.0 RNA assay, *Methods Mol. Biol.* 2857 (2025) 89–98.
- [53] C. Dullin, F. di Lillo, A. Svetlove, J. Albers, W. Wagner, A. Markus, et al., Multiscale biomedical imaging at the SYRMEP beamline of Elettra - closing the gap between preclinical research and patient applications, *Physics Open* 6 (2021).
- [54] A. Gianoncelli, G. Sena Souza, G. Kourousias, E. Pascotto, P. Tafforeau, E. Longo, et al., Morphological and chemical investigation of ovarian structures in a bovine model by contrast-enhanced X-ray imaging and microscopy, *Int. J. Mol. Sci.* 24 (2023).
- [55] F. Brun, L. Massimi, M. Fratini, D. Drossi, F. Bille, A. Accardo, et al., SYRMEP Tomo Project: a graphical user interface for customizing CT reconstruction workflows, *Adv. Struct. Chem. Imaging* 3 (2017) 4.
- [56] D. Paganin, S.C. Mayo, T.E. Gureyev, P.R. Miller, S.W. Wilkins, Simultaneous phase and amplitude extraction from a single defocused image of a homogeneous object, *J. Microsc.* 206 (2002) 33–40.
- [57] J.M. Palacios-Jaraquemada, A. Nieto-Calvache, N.A. Basanta, Anatomical basis for the uterine vascular control: implications in training, knowledge, and outcomes, *Am. J. Obstet. Gynecol. MFM* 5 (2023) 100953.
- [58] J.D. Asseler, J.S. Del Valle, S.M. Chuva de Sousa Lopes, M.O. Verhoeven, M. Goddijn, J.A.F. Huirne, et al., One-third of amenorrheic transmasculine people on testosterone ovulate, *Cell. Rep. Med.* (2024), <https://doi.org/10.1016/j.xcrm.2024.101440>.
- [59] X. Xu, L. Mu, L. Li, J. Liang, S. Zhang, L. Jia, et al., Imaging and tracing the pattern of adult ovarian angiogenesis implies a strategy against female reproductive aging, *Sci. Adv.* 8 (2022) eabi8683.
- [60] A. Guzman, C.G. Hernandez-Coronado, C.G. Gutierrez, A.M. Rosales-Torres, The vascular endothelial growth factor (VEGF) system as a key regulator of ovarian follicle angiogenesis and growth, *Mol. Reprod. Dev.* 90 (2023) 201–217.
- [61] R. Abir, A. Ao, X.Y. Zhang, R. Garor, S. Nitke, B. Fisch, Vascular endothelial growth factor A and its two receptors in human preantral follicles from fetuses, girls, and women, *Fertil. Steril.* 93 (2010) 2337–2347.



- [62] G. Huang, F. Li, X. Zhao, Y. Ma, Y. Li, M. Lin, et al., Functional and biomimetic materials for engineering of the three-dimensional cell microenvironment, *Chem. Rev.* 117 (2017) 12764–12850.
- [63] J.C. Fontoura, C. Viezzer, F.G. Dos Santos, R.A. Ligabue, R. Weinlich, R.D. Puga, et al., Comparison of 2D and 3D cell culture models for cell growth, gene expression and drug resistance, *Mater. Sci. Eng., C* 107 (2020) 110264.
- [64] J. Zhang, M.P. Schwartz, Z. Hou, Y. Bai, H. Ardalani, S. Swanson, et al., A genome-wide analysis of human pluripotent stem cell-derived endothelial cells in 2D or 3D culture, *Stem Cell Rep.* 8 (2017) 907–918.
- [65] B. Wang, R. Chen, H. Gao, X. Lv, L. Chen, W. Wang, et al., A comparative study unraveling the effects of TNF-alpha stimulation on endothelial cells between 2D and 3D culture, *Biomed Mater* 15 (2020) 065018.
- [66] G. Akiri, D. Nahari, Y. Finkelstein, S.Y. Le, O. Elroy-Stein, B.Z. Levi, Regulation of vascular endothelial growth factor (VEGF) expression is mediated by internal initiation of translation and alternative initiation of transcription, *Oncogene* 17 (1998) 227–236.
- [67] M. Spazzapan, S. Pegoraro, C. Agostinis, R. Bulla, The role of complement component C1q in angiogenesis, *Explor. Immunol.* (2023) 574–589, <https://doi.org/10.37349/ei.2023.00122>.
- [68] P. Vuorela, E. Hatva, A. Lymboussaki, A. Kaipainen, V. Joukov, M.G. Persico, et al., Expression of vascular endothelial growth factor and placenta growth factor in human placenta, *Biol. Reprod.* 56 (1997) 489–494.
- [69] Falco S. De, The discovery of placenta growth factor and its biological activity, *Exp. Mol. Med.* 44 (2012) 1–9.
- [70] C. Gu, E. Giraudo, The role of semaphorins and their receptors in vascular development and cancer, *Exp. Cell Res.* 319 (2013) 1306–1316.
- [71] T. Matsumoto, L. Claesson-Welsh, VEGF receptor signal transduction, *Sci. STKE* 2001 (2001) re21.
- [72] S. Chakrabarti, K.D. Patel, Matrix metalloproteinase-2 (MMP-2) and MMP-9 in pulmonary pathology, *Exp. Lung Res.* 31 (2005) 599–621.
- [73] A. Nikolov, N. Popovski, Role of gelatinases MMP-2 and MMP-9 in healthy and complicated pregnancy and their future potential as preeclampsia biomarkers, *Diagnostics* 11 (2021).
- [74] M.P. Caley, V.L. Martins, E.A. O'Toole, Metalloproteinases and wound healing, *Adv. Wound Care* 4 (2015) 225–234.
- [75] S. Quintero-Fabian, R. Arreola, E. Becerril-Villanueva, J.C. Torres-Romero, V. Arana-Argaez, J. Lara-Riegos, et al., Role of matrix metalloproteinases in angiogenesis and cancer, *Front. Oncol.* 9 (2019) 1370.
- [76] H. Roness, D. Meirou, Follicle reserve loss in ovarian tissue transplantation, *Reproduction* 158 (2019) F35–F44.
- [77] A. Grada, J. Mervis, V. Falanga, Research techniques made simple: animal models of wound healing, *J. Invest. Dermatol.* 138 (2018), 2095–20105 e1.
- [78] R. Soleimani, J. Van der Elst, E. Heytens, R. Van den Broecke, J. Gerris, M. Dhont, et al., Back muscle as a promising site for ovarian tissue transplantation, an animal model, *Hum. Reprod.* 23 (2008) 619–626.
- [79] A.S. Van Eyck, C. Bouzin, O. Feron, L. Romeu, A. Van Langendonck, J. Donnez, et al., Both host and graft vessels contribute to revascularization of xenografted human ovarian tissue in a murine model, *Fertil. Steril.* 93 (2010) 1676–1685.
- [80] Adrados C. Subiran, H.O. Olesen, S.V. Olesen, S.E. Pors, S. Holtze, T. Hildebrandt, et al., Exploring the effect of platelet-rich plasma on vascularization and survival of follicles in xenotransplanted human ovarian tissue, *Reprod. Biomed. Online* 49 (2024) 104274.
- [81] S.G. Kristensen, H.O. Olesen, M.C. Zeuthen, S.E. Pors, C.Y. Andersen, L. S. Mamsen, Revascularization of human ovarian grafts is equally efficient from both sides of the cortex tissue, *Reprod. Biomed. Online* 44 (2022) 991–994.
- [82] A. Kedem, A. Aelion-Brauer, P. Guo, D. Wen, B.S. Ding, R. Lis, et al., Activated ovarian endothelial cells promote early follicular development and survival, *J. Ovarian Res.* 10 (2017) 64.
- [83] M.W. Laschke, M.D. Menger, Vascularization in tissue engineering: angiogenesis versus inosculation, *Eur. Surg. Res.* 48 (2012) 85–92.
- [84] D.D. Manavella, L. Cacciottola, S. Pomme, C.M. Desmet, B.F. Jordan, J. Donnez, et al., Two-step transplantation with adipose tissue-derived stem cells increases follicle survival by enhancing vascularization in xenografted frozen-thawed human ovarian tissue, *Hum. Reprod.* 33 (2018) 1107–1116.
- [85] K. Fazelian-Dehkordi, T. Talaei-Khozani, S.F.M. A. Three-dimensional in vitro maturation of rabbit oocytes enriched with sheep decellularized greater omentum, *Vet. Med. Sci.* 8 (2022) 2092–2103.
- [86] A.Y. Shen, W.M. Rozen, A. Polyakov, K. Stern, G. Rozen, Applying plastic surgery principles to ovarian tissue transplantation, *Gland Surg.* 10 (2021) 2266–2274.
- [87] R. Abir, D. Stav, Y. Taieb, R. Gabbay-Benziv, M. Kirschner, A. Ben-Haroush, et al., Novel extra cellular-like matrices to improve human ovarian grafting, *J. Assist. Reprod. Genet.* 37 (2020) 2105–2117.
- [88] M. Konno, A. Hamabe, S. Hasegawa, H. Ogawa, T. Fukusumi, S. Nishikawa, et al., Adipose-derived mesenchymal stem cells and regenerative medicine, *Dev. Growth Differ.* 55 (2013) 309–318.
- [89] Y. Qin, G. Ge, P. Yang, L. Wang, Y. Qiao, G. Pan, et al., An update on adipose-derived stem cells for regenerative medicine: where challenge meets opportunity, *Adv. Sci. (Weinh.)* 10 (2023) e2207334.
- [90] J. Cheng, X. Ruan, Y. Li, J. Du, F. Jin, M. Gu, et al., Effects of hypoxia-preconditioned hucMSCs on neovascularization and follicle survival in frozen/thawed human ovarian cortex transplanted to immunodeficient mice, *Stem Cell Res. Ther.* 13 (2022) 474.
- [91] M.M. Dolmans, L. Cacciottola, C.A. Amorim, D. Manavella, Translational research aiming to improve survival of ovarian tissue transplants using adipose tissue-derived stem cells, *Acta Obstet. Gynecol. Scand.* 98 (2019) 665–671.
- [92] D.D. Manavella, L. Cacciottola, V.L. Payen, C.A. Amorim, J. Donnez, M. M. Dolmans, Adipose tissue-derived stem cells boost vascularization in grafted ovarian tissue by growth factor secretion and differentiation into endothelial cell lineages, *Mol. Hum. Reprod.* 25 (2019) 184–193.
- [93] W.Z. Ma, X.M. Zheng, C.C. Hei, C.J. Zhao, S.S. Xie, Q. Chang, et al., Optimal FSH usage in revascularization of allotransplanted ovarian tissue in mice, *J. Ovarian Res.* 10 (2017) 5.
- [94] L. Wang, Y.F. Ying, Y.L. Ouyang, J.F. Wang, J. Xu, VEGF and bFGF increase survival of xenografted human ovarian tissue in an experimental rabbit model, *J. Assist. Reprod. Genet.* 30 (2013) 1301–1311.
- [95] J. Gao, Y. Huang, M. Li, H. Zhao, Y. Zhao, R. Li, et al., Effect of local basic fibroblast growth factor and vascular endothelial growth factor on subcutaneously allotransplanted ovarian tissue in ovariectomized mice, *PLoS One* 10 (2015) e0134035.
- [96] L. Henry, S. Labied, M. Fransolet, N. Kirschvink, S. Blacher, A. Noel, et al., Isoform 165 of vascular endothelial growth factor in collagen matrix improves ovine cryopreserved ovarian tissue revascularisation after xenotransplantation in mice, *Reprod. Biol. Endocrinol.* 13 (2015) 12.
- [97] J. Su, L. Ding, J. Cheng, J. Yang, X. Li, G. Yan, et al., Transplantation of adipose-derived stem cells combined with collagen scaffolds restores ovarian function in a rat model of premature ovarian insufficiency, *Hum. Reprod.* 31 (2016) 1075–1086.
- [98] M. Saccomano, J. Albers, G. Tromba, M. Dobrivojevic Radmilovic, S. Gajovic, F. Alves, et al., Synchrotron inline phase contrast microCT enables detailed virtual histology of embedded soft-tissue samples with and without staining, *J. Synchrotron Radiat.* 25 (2018) 1153–1161.
- [99] M. Fratini, I. Bukreeva, G. Campi, F. Brun, G. Tromba, P. Modregger, et al., Simultaneous submicrometric 3D imaging of the micro-vascular network and the neuronal system in a mouse spinal cord, *Sci. Rep.* 5 (2015) 8514.
- [100] F. Palermo, N. Pieroni, A. Sanna, B. Parodi, C. Venturi, G. Begani Provinciali, et al., Multilevel X-ray imaging approach to assess the sequential evolution of multi-organ damage in multiple sclerosis, *Commun. Phys.* 5 (2022).
- [101] J. Albers, W.L. Wagner, M.O. Fiedler, A. Rothermel, F. Wunemann, F. Di Lillo, et al., High resolution propagation-based lung imaging at clinically relevant X-ray dose levels, *Sci. Rep.* 13 (2023) 4788.
- [102] C.L. Walsh, P. Tafforeau, W.L. Wagner, D.J. Jafree, A. Bellier, C. Werlein, et al., Imaging intact human organs with local resolution of cellular structures using hierarchical phase-contrast tomography, *Nat. Methods* 18 (2021) 1532–1541.
- [103] P. Cloetens, R. Barrett, J. Baruchel, J.P. Guigay, M. Schlenker, Phase objects in synchrotron radiation hard x-ray imaging, *J. Phys. Appl. Phys.* 29 (1996) 133.
- [104] A. Bravin, P. Coan, P. Suortti, X-ray phase-contrast imaging: from pre-clinical applications towards clinics, *Phys. Med. Biol.* 58 (2013) R1–R35.
- [105] L. Pascolo, G. Sena, A. Gianoncelli, A. Cernogoraz, G. Kourousias, B.D. Metscher, et al., Hard and soft X-ray imaging to resolve human ovarian cortical structures, *J. Synchrotron Radiat.* 26 (2019) 1322–1329.